EXAMINING THE ROLE OF DISCHARGE GAS AND VAPOUR INTRODUCTION FOR ATMOSPHERIC PRESSURE PHOTOIONIZATION MASS SPECTROMETRY

by

Davin Martin Richard Carter

B. Sc., Carleton University, 2006

A THESIS SUBMITTED IN PARTIAL FULFILLMENT OF

THE REQUIREMENTS FOR THE DEGREE OF

MASTER OF SCIENCE

in

THE COLLEGE OF GRADUATE STUDIES

(Chemistry)

THE UNIVERSITY OF BRITISH COLUMBIA

(Okanagan)

June 2012

Abstract

The recent introduction of commercial Atmospheric Pressure PhotoIonization (APPI) sources for use on Liquid Chromatography-Mass Spectrometry (LCMS) instruments has expanded the range of analytes that can be analyzed to include non-polar compounds. The two commercial photon sources use a low pressure krypton discharge lamp that selectively ionizes many classes of analytes but not common solvents. This thesis explores two hypotheses; (a) that ionization can be independent of discharge gas type and (b) that vapours of solid samples can be ionized and rapidly analyzed by mass spectrometry.

To explore the effect of discharge gas on ionization, a novel atmospheric pressure discharge lamp was constructed. Helium, nitrogen, argon, hydrogen, oxygen, carbon dioxide, and compressed air were evaluated as discharge gases to generate photons that would induce photoionization in naphthalene as a representative polycyclic aromatic hydrocarbon. Photon emission spectra of argon, helium, hydrogen, oxygen and nitrogen were characterized and found to be consistent to reference spectra. Calibration curves were constructed for naphthalene and compared to a calibration curve obtained using a commercial (PhotoMate, Syagen Inc.) photoionization lamp. The custom made discharge lamp was slightly more sensitive and gave mass spectra comparable to the commercial lamp leading to the conclusion that ionization was independent of discharge gas type.

Under the second objective, an innovative way to introduce vapours from solid samples was developed. Small amounts of solid crystal sample were heated to produce vapours that were then photoionized. Mass spectra were collected on a number of polycyclic aromatic compounds and metal containing organic compounds. Collision induced dissociation was used to characterize specific analytes of interest.

The ability to use a variety of discharge gases for photoionization lowers the cost of construction and improves the ruggedness of photoionization ionization sources. The ability to quickly characterize solid samples has a range of applications including rapid confirmation of synthetic chemistry reactions, quality assurance in pharmaceutical production, detection of drugs of abuse and detection of chemical warfare agents.

Preface

This thesis is in part the result of collaborations with the Institute for Pure and Applied Mass Spectrometry at the University of Wuppertal, Germany. Design, fabrication and evaluation of the Lightning Ion Source was a joint effort of Dr. Hendrik Kersten and myself. I primarily designed, fabricated and evaluated the TAVI apparatus with some assistance from Dr. Kersten.

Portions of this work have been presented at the American Society for Mass Spectrometry conference in 2010 and the International Conference on Analytical Sciences and Spectroscopy in 2009.

Table of Contents

List of Tables

List of Figures

Acknowledgements

A sincere thank you to Dr. Rob O'Brien for supervising and guiding me through this process. Throughout the process Rob has given me incredible insights and advice.

I wish to thank the many people who have helped and encouraged me throughout this research. The staff of the UBC Okanagan Chemistry Department were of great help during my thesis. I'd like to acknowledge a passionate educator, Judit Moldovan, who was an inspiration for educators. The time and useful feedback from my thesis committee has been incredibly useful throughout this project. Dave Arkinstall was a great sounding board and wealth of experience. Life long friends, Dr. Thorsten Benter and Dr. Hendrik Kersten of the Institute for Pure and Applied Mass Spectrometry from the University of Wuppertal, Germany provided great discussions and ideas for this research.

I'd like to acknowledge the support my parents and brother have given over the years. Sadly, my father in law, who had a keen curiosity and interest in science, passed away days before my defense. The patience, support and support of my wife made all this work possible.

This work was made possible by instrumentation grants from the Western Economic Diversification fund and The British Columbia Knowledge Development fund.

Chapter 1: Introduction

Photons were one of the first energy sources used to generate ions for mass spectrometry (Ditchburn and Arnot, 1929). Despite that fact, photoionization sources were not widely used for quantitative mass spectrometry until the year 2000 when Atmospheric Pressure Photoionization (APPI) sources were introduced for use on Liquid Chromatography-Mass Spectrometer (LCMS) instruments (Robb et al., 2000; Syage et al., 2000). There are two distinct patented commercially available sources: The PhotoMate™ source based on the Syage patent (Syage et al., United States, 5,808,299, 1998) is available from Syagen Technology and the PhotoSpray™ (Robb et al., United States, 6,534,765 B1, 2003), is available from MDS Sciex. In both cases, a low pressure krypton discharge lamp is used as the photon source.

The APPI-LCMS systems that are currently in operation are used primarily to measure analytes in solution. It has been demonstrated that the analyte vapors in the absence of solvents, analyzed by APPI, primarily produced molecular ion mass spectra (Syage, J., 2004). From this we generated a hypothesis that examining the vapors from materials produced by synthetic organic processes could provide key diagnostic information. The validity of this hypothesis will also be explored in this work. We also investigate the use of an alternate discharge lamp to generate photons for an APPI-LCMS system.

This introduction will begin with background material on the history of photon generation and also include an explanation of photon generation. A summary of the history of

photoionization mass spectrometry is then provided, then a description of optical filters and an alternate technique, photoelectron spectroscopy, that provides insight into photoionization mechanisms. These lead into a summary of the current understanding of reaction mechanisms occurring in APPI – MS. Our understanding of these mechanisms enabled us to hypothesize that APPI MS could be extremely useful for structure determination for synthetic compounds and this led to the development of the heated probe introduction approach that we will also cover at the end of this introduction. A brief summary of rapid ambient ionization analysis techniques is then offered.

1.1 History of photon generation

The production of photons is a fundamental part of photoionization and has been studied for over 100 years (Lyman, 1906). The photoemission spectra of many gases have shown extensive emission lines (Lyman, 1906; Hopfield, 1930, Tanaka et al., 1958). Many of the original measurements of photoemission spectra were carried out with open flow discharge cells operating near one atmosphere with large monochromators and large arrays of photographic plates (Lyman and Saunders, 1926; Hopfield, 1930).

Electrical discharges of many gases have been found to produce photons over a wide range of energies. Beginning in 1906, a number of researchers measured the emission wavelengths of hydrogen and helium. A significant number of hydrogen line emissions were identified from 100 nm to 185 nm (Lyman, 1906; Lyman, 1924; Millikan and Bowen, 1924; Banning, 1942; Poschenrieder and Warneck, 1968) and major emission lines of helium were found at

25.63, 30.36 and 58.44 nm with continuous emission between 60.0 nm and 100.0 nm (Hopfield, 1930; Huffman et al., 1965).

Other elements have been found to have numerous emission lines. For example, over eighty emission lines were attributed to carbon within the wavelength range of 36 nm to 180 nm, fourteen to nitrogen between 66 nm and 150 nm and sixty eight to oxygen ranging from 14 nm and 134 nm (Millikan and Bowen, 1924). Xenon was found to have a broad continuous discharge from 150 to 210 nm (Wilkinson and Tanaka, 1955; Tanaka, 1955, Huffman et al., 1965). Krypton was found to have a continuum emission starting at its resonance line at 123.6 nm extending to 180.0 nm (Tanaka, 1955; Huffman et al., 1965). The argon continuum was found to range from 105.0 to 155.0 nm (Lyman, 1925; Huffman et al., 1965; Tanaka, 1955). It is especially noteworthy that electrical discharges in air have been found to release photons of continuous energy between 45 nm and 240 nm (Sabine, 1939) corresponding to energies between 27.5 eV and 5.1 eV, which covers the full range of photoionization. These and other reports from the literature show that many discharge gases produce photons of varying energies.

Emission spectra have been found to be dependent on several parameters; gas pressure within the discharge chamber, electrode gap, electrode material and trace contaminants (Druyvestevyn and Penning, 1940; Huffman et al.,1965; Tanaka, 1955; Tanaka et al., 1958). Varying pressure has been found to broaden emission lines, shift emission lines and cause asymmetry in emission lines (Lalos and Hammond, 1961).

While much of the literature focuses on the strongest emission lines, emission spectra have been shown to have broad ranges of photon wavelengths (Tanaka et al., 1958). It has been shown that hydrogen, krypton, argon and helium have broad emission peaks that are 30 nm to 50 nm in width.

1.2 Krypton photon generation

The most commonly used photoionization lamp is a krypton discharge lamp. As with all such discharge sources, the photon energies and related wavelengths are characteristic of the discharge gas used (Gross and Caprioli, 2007). In the initial publications describing APPI LCMS (Robb et al., 2000, Syage et al., 2000) it was stressed that the selection of lamp wavelength was critically important. The krypton discharge lamp was selected because its emission spectra allowed ionization of an important range of analytes. In a low pressure krypton discharge lamp, the most significant photons produced have energies of 10.0 eV (80%) or 10.6 eV (20%) (Borsdorf et al., 2007) that are sufficient to ionize important analyte classes such as steroids and other aromatic analytes but below the ionization potential of most LC solvents.

The mechanism for photon emission within a discharge lamp begins with a discharge of electrons from the electrode surface through the low pressure gas contained within the lamp. Typical voltages present within these devices are approximately 400 volts. The energy from the discharge of electrons through the low pressure krypton gas generates a population of krypton cations and free electrons. These rapidly recombine to form excited state krypton

atoms that relax to common metastable states (Kr*). These states are called metastable states because they are known to persist for long periods of time since they are in triplet spin state while the ground state is a singlet state. These metastable states do eventually relax back to the ground state and release photons of well defined energies. An analogous process occurs in all noble gasses. This process of photon is described in Equations 1a through 1c below.

$e^- + Kr \rightarrow Kr^+ + 2e^-$ **Equation 1a**
$Kr^+ + e^- \rightarrow Kr^*$ **Equation 1b**
$Kr^* \rightarrow Kr + h\nu$ **Equation 1c**

1.3 History of photoionization mass spectrometry

Photoionization mass spectrometry began in 1929 (Ditchburn and Arnot, 1929) and has examined variety of discharge gases to produce photons with a wide range of energies (Webb, United States Patent, 3,521,054, 1970). The first generation of photo-induced ions was first reported in 1929 by Ditchburn and Arnot, who used a magnetic sector mass spectrometer to detect potassium photo-induced ions (Ditchburn and Arnot, 1929). Lossing and Tanaka (1956) published mass spectra of parent ions of acetone, anisole and various hydrocarbons generated with a sector mass spectrometer using a krypton discharge lamp with a lithium fluoride window. The essentially monochromatic nature of photons from their lamp offered sharp separation of ion-forming processes and great simplification of photoionization spectra over traditional electron impact that often exhibited many fragment peaks and weak molecular ion peak (Lossing and Tanaka, 1956). Herzog and Marmo (1957) described a hydrogen discharge and lithium fluoride window that produced very simple mass spectra

usually consisting of just the molecular ion peak. Jensen and Libby (1964) constructed a simple helium discharge lamp that used tungsten wires as electrodes. They investigated discharge current, electrode temperature (up to 1660 k) and charge density around the electrodes at different orientations (Jensen and Libby, 1964). In 1966, photoionization mass spectra with little fragmentation was observed and it was found that the parent or "parent plus one" was the sole contributor to the mass spectrum (Poschenrieder and Warneck, 1966). Using different discharge chamber capillaries, made of quartz (emitting a continuous flux) and ceramic (emitting a pulsed discharge), coupled with a monochrometer, emission bands from various gases with a resolution of 0.1 eV were produced (Poschenrieder and Warneck, 1966). By selection of discharge gas, the wavelength of resulting photons could be controlled to selectively ionize the gases of trace analyte while not ionizing interfering gases. This allowed for analysis of trace gases like N_2O that would have been masked by CO_2 and allowed separation of CO from N_2 (Poschenrieder and Warneck, 1966). The elimination of a heated filament that may cause thermal degradation was seen as an additional benefit of photoionization (Poschenrieder and Warneck, 1968). In 1966, Brion reported a windowless photoionization source for use with a solid sample probe that showed large increases in relative abundance of molecular ion in comparison to traditional electron impact ionization source (Brion, 1966). In a 1969 patent, Yamane described a photoionization detector that used a discharge in helium, argon or hydrogen to measure gases and vapours (Yamane, United States Patent, 3,454,828, 1969). A 1970 patent from NASA used a continuous wavelength argon source and a diffraction grating to provide a selectable wavelength photo ionization source (Webb, United States Patent, 3,521,054, 1970). A patent was issued to Driscoll for a selective photoionization source (Driscoll, United States Patent, 40,359/72,

1972). Using gases ranging from hydrogen, xenon, argon or krypton resulted in photons of energies between 9.25 to 15.55 eV were transmitted either through a lithium or magnesium fluoride window. The first report of a photoionization detector (PID) coupled to GC was in the 1970's when Driscoll et al. replaced their traditional FID detector with a PID. In their work, a variety of hydrocarbons were ionized via a sealed UV lamp that emitted 10.20 eV photons from a hydrogen discharge through a magnesium fluoride window (Driscoll and Warneck, 1973). Driscoll recognized that fragmentation of analytes and interfering matrix could be minimized by controlling photon energy (Driscoll and Warneck, 1973). Unlike, conventional electron impact mass spectrometry at the time, they were able to differentiate oxygen gas from methanol by selecting a photon wavelength that ionized methanol but not oxygen (Driscoll and Warneck, 1973). In 1991, Revel'skii et al. proposed using photoionization mass spectrometry without separation of multi component mixtures. Examining low molecular weight compounds, the group examined esters, alkanes, alkenes, ketones and aromatic hydrocarbons using photons from a krypton discharge lamp at 10.2 eV and detected them with a mass spectrometer (Revel'skii et al. 1991). The literature contains extensive work developing and using photoionization prior to 2000.

1.4 Discharge windows

Discharge windows allow selective transmission of certain light wavelengths while holding back the discharge gas and the complex discharge induced chemistry (ions and metastables) (Druyvesteyn, 1940; Kiser, 1965). When lithium fluoride is used as a discharge window, photons of wavelength greater than 105 nm (11.8 eV) can pass through to reach the analytes (Gerisimova, 2006). The transmission properties of various materials has been studied for over 100 years (Lyman. 1906).

The study of optical transmission of a variety of substances began with Lyman. Windows of fluorite (CaF_2) were used by Lyman in his 1906 examination of hydrogen discharge lines where he observed no emission lines less than 120 nm were transmitted through the fluorite. He wrote that the "discovery of some substance transparent to light of the very shortest wave-length known to exist would be an important step" (Lyman, 1906). Further investigation found that fluorite allows transmission of photons on energies 115 nm to 700 nm (Gerasimova, 2006). Examinations into the UV-optical properties of sodium and potassium date back to 1919 when Wood found that thin layers of potassium did not transmit any visible light but transmitted at UV wavelengths less than 360 nm (Wood, 1919). The optical properties of lithium fluoride in the extreme ultraviolet were first reported in 1927 (Gyulai, 1927). A more detailed study compared lithium fluoride to calcium fluorite (CaF_2) and found that LiF was more transparent in the far UV (Schneider, 1936) transmitting light of wavelengths down to 110 nm, (Gyulai, 1927; Schneider, 1936; Milgram and Givens, 1962; Patterson and Vaughn, 1963; Gerasimova, 2006). Later, the UV cutoff was further refined to

105 nm (11.8 eV) (Kato and Nakashima,1960; Kato, 1961). It was noted that there should be sufficient separation between electrical discharges and LiF windows to avoid discolouration of the window (Schneider, 1936). Magnesium fluoride has also been used for photo ionization lamps (Robb, United States Patent, 6,534,765 B1, 2003) and has been reported to be slightly more tolerant of harsh conditions and transmit photons of 110.0 - 136.0 nm wavelength (Duncanson and Stevenson, 1958; Gerasimova, 2006). Aluminum thin layers have been used as filters and windows in the extreme UV (Hass and Tousey, 1959; Madden and Canfield, 1961). Thin aluminum foil transmits up to 100 nm (Jenson and Libby, 1964; Walker et al., 1958; Kinsinger et al., 1972; Sieck and Gordon, 1973).

1.5 Photoelectron spectroscopy

Photoelectron spectroscopy (PES) measurements offer information about atomic and molecular energy levels (Nordling et al., 1957; Frost et al., 1966) and provide important insights into photoionization. PES describes that if photon energy is in excess of the ionization potential, ionization will likely occur as described by Equation 2.

$$E_{electron} = h\nu - E_{ionization\ potential}$$ **Equation 2:** Electron energy

PES measures the energy of electrons emitted from material exposed to high energy photons. The kinetic energy of photoelectrons can be measured by an electrostatic kinetic energy analyzer coupled to an electron multiplier. Typically, a microwave powered helium discharge is used to produce monochromatic photons at 58.4 nm or 21.2 eV (Kinsinger et al., 1972).

The energy of a photon is related to Plank's constant (*h*), the speed of light (c) and its wavelength (ν) and the energy in excess of the ionization potential leaves in the departing electron as given by Equation 1. The generation of photoelectrons was first observed by Heinrich Hertz in 1887 and explained by Albert Einstein in quantum mechanical terms when he developed the theory that light was composed of discrete quanta, or photons (Einstein, 1905).

It has been shown that electrons of differing binding energies can be removed by high energy photons (Kinsinger et al., 1972). In larger molecules, the release of electrons of differing ionization potentials gives rise to ionization continua with many peaks (Al-Joboury and Turner, 1963; Clark and Frost, 1967).

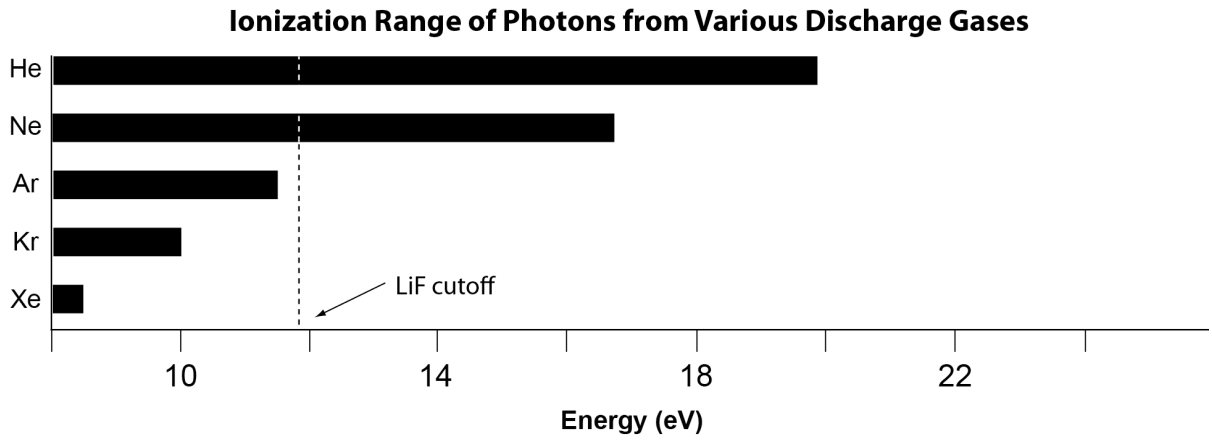

Figure 1: Relation between photon energy and discharge gas

All of the of the noble gases listed in Figure 1, with the exception of xenon, have sufficient energy to ionize benzene. Photons derived from a helium discharge have the greatest energy at 19.8 eV and could induce various cationic states. Photons from krypton discharges are used in commercial APPI discharge lamps as their energy is below most solvents but above most analyte molecules (Robb et al., 2000). The photon cut off for lithium fluoride crystals is indicated in Figure 1 to highlight that lithium fluoride is not useful for photons with energy greater than 11.8 eV (or less than 105 nm).

1.6 Mechanisms of photoionization

Ions found in photoionization mass spectra can generally be attributed to two distinct but related mechanisms. From photoelectron theory, direct photoionization would be the expected to only produce molecular ion and a free electron. However, the enhancement of the signal through the addition of dopants leads to the generation of non-molecular ions such as $(M+H)^+$ that are a clear demonstration of chemical processes are involved (Syage, 2004) or in other words photoinduced chemical ionization.

1.6.1 Mechanism of direct photoionization

By definition, primary photoionization leads exclusively to a molecular cation M^+, and direct PI spectra are dominated by a molecular cation peak (Gross et al., 2007) that is produced as described in Equation 3. Unlike other ionization methods, the photoionization process does not lead to deposition of excess energy into the molecule. From photoelectric theory, all of

the excess photon energy is deposited into the departing electron (Equation 3) and thus the only excess energy that the molecular ion will have is a function of the geometric differences between the neutral and the specific cation state produced. In many cases there is very little difference in ground state geometries and so little fragmentation of parent ions is observed. This makes APPI a soft ionization technique resulting in predominately molecular ions (Syage et al., 2004). As photoionization involves interactions of photons with compounds, gas phase acid base chemistry plays a much smaller role as compared to ESI and APCI (Bos et al., 2006).

$$M + h\nu \rightarrow M^+ + e^-$$ **Equation 3:** Photoionization

1.6.2 Mechanisms of secondary ionization leading to $[M+H]^+$

The photoionization mechanism described by the previous equation can only produce simple molecular ions or fragments but it has been widely noted that a majority of ions generated by the commercial APPI sources are $[M+H]^+$ rather than M^+ (Syage et al., 2004). The formation of $[M+H]^+$ has been demonstrated to be a result of "chemical ionization" that involves solvent or matrix species in some form but the mechanism of ionization is disputed (Kaupilla et al., 2002; Syage et al., 2004).

It is highly probable that the reactions that lead to $[M+H]^+$ are the result of a chemical ionization process involving solvent or other matrix species that have been chemically activated by photon absorption or reactions resulting from photon absorption leading to

Photon Induced Chemical Ionization (PICI) (Kersten et al., 2009). Nevertheless, the specific mechanisms of formation of $[M+H]^+$ are not fully understood and several different mechanisms have been proposed (Kaupilla et al., 2002; Syage et al., 2004; Kersten et al., 2009). One hypothesis proposed is analyte cation formation followed by hydrogen abstraction from protic solvents (Syage et al., 2004). Kaupilla, in 2002, examined ionization mechanisms of APPI and concluded that $[M+H]^+$ is most likely the result of proton transfer from the protonated solvent to the analyte. Interestingly, Kauppila disregarded direct photoionization for the formation of M^+ and believed that M^+ is formed primarily by charge exchange between $C_7H_8^{\bullet+}$ and the analyte (Kauppila et al., 2002). Others hypothesize that the significant amount of neutral radicals are produced by the krypton discharge lamp and that these could have a significant influence on APPI spectra (Kersten et al., 2009).

By examining several naphthalenes of varying proton affinities Kauppila et al. (2002) found that toluene radical cation was formed by photoionization as described in Equation 4. If the proton affinity of the solvent was greater than benzyl radical, proton transfer is possible leading to possible dopant- solvent- analyte cascade of proton transfer. Two different mechanisms are described below, both resulting in the formation of $[M+H]^+$.

<u>Formation of $[A+H]^+$ via dopant charge transfer</u> (Kauppila et al., 2002)

$h\nu + C_7H_8 \rightarrow C_7H_8^{\bullet+} + e^-$ **Equation 4:** Toluene dopant radical cation formation

$C_7H_8^{\bullet+} + M \rightarrow C_7H_7^{\bullet} + MH^+$ **Equation 5:** Proton transfer between dopant & analyte

Formation of $[A+H]^+$ via dopant charge transfer to solvent to analyte (Kauppila et al., 2002)

$h\nu + C_7H_8 \rightarrow C_7H_8^{\bullet+} + e^-$	**Equation 6:** toluene dopant radical cation formation
$C_7H_8^{\bullet+} + S \rightarrow C_7H_7^{\bullet} + SH^+$	**Equation 7:** proton transfer between dopant & solvent
$SH^+ + M \rightarrow MH^+ + S$	**Equation 8:** formation of AH^+ via solvent charge transfer

In contrast, Syage et al. (2004) reported direct analyte photoionization followed by hydrogen abstraction from solvent to form $[M+H]^+$. By comparing spectra of pure vapours to solvated samples and comparing spectra of protic and aprotic solvents, Syage et al. (2004) concluded that the solvents were the source of protons. The mechanism of $[M+H]^+$ formation was assessed in a comparison of mass spectra of pure vapours to the spectra of analytes dissolved in various solvents and found that M^+ dominated in headspace vapours (Syage et al., 2004). The presence of $[M+H]^+$ ions only in solvated samples indicates the involvement of the solvent in formation of $[M+H]^+$. Further supporting that the proton came from the solvent was evidence that $[M+H]^+$ formed in the presence of protic solvents while $[M+H]^+$ wasn't observed to the same extent with aprotic solvents. Examination of the ratio of $[M+H]^+/M^+$ over a range of concentrations provided evidence that self reaction was not significant reaction pathway (Syage et al., 2004). Further examination indicated the formation of $[M+H]^+$ in the ionization chamber rather than inside the mass spectrometer. It was also demonstrated that the $[M+H]^+/M^+$ ratio is highly dependent on experimental parameters that affect ion residence time in the ionization chamber. Modelling studies indicated that proton affinity was a good proxy for the degree of hydrogen addition, whereas ionization energy was found not to be a good indicator (Syage et al., 2004).

$M + h\nu \rightarrow M^+ + e^-$ **Equation 2**: Photoionization

$M^+ + S \rightarrow MH^+ + S\text{-}H$ **Equation 9:** PICI proton abstraction from protic solvent

1.6.3 Dopants

To increase the likelihood of analyte ionization, a chemical can be doped into the reaction chamber to act as a charge carrier. In one of the original APPI papers, it was hypothesized that direct photoionization leading to molecular cation ion radical was quite low but that use of a dopant such as toluene or acetone can greatly increase ion production (Robb et al., 2000).

High collision frequency at atmospheric pressures results in a short mean free path of ions of 6.5×10^{-6} cm (Kauppila et al., 2002). Lorenz et al. (2008) reported that an ion generated ten millimetres from the intake nozzle typically experiences 10^8 collisions in the 15 ms it takes to enter the nozzle. Additionally, at atmospheric pressure, the probability of a photon hitting an analyte molecule, before the photon is quenched, is low. It has been found that intensity of light drops to 2% after traveling only 3.5 millimetres (Lorenz et al., 2008).

Equations 7 and 8 describe charge transfer between a dopant and an analyte molecule. In dopant assisted atmospheric pressure photoionization (DA-APPI), ionization efficiency is dependent on proton affinity (Robb et al., 2000) similar to the mechanisms of ESI and APCI (Syage et al., 2004).

Toluene has been found to be a good dopant that is attributed to its ability to form a stable seven membered tropylium cation, $C_7H_7^+$ (Syage et al., 2004). Ironically, the reason for choosing a krypton lamp is to selectively ionize the analytes and not the matrix but dopant assisted photoionization purposely ionizes a compound that is part of the matrix in significant quantities (up to 15% (Raffaelli and Saba, 2003)) to act as an ionizing agent.

1.7 Structure determination

Structure determination is an important piece of information in the determination of new synthetic pathways and mechanisms (Eelman et al., 2008). Strategies have been developed to characterize organometallic compounds with mass spectrometric techniques, however, many of these have limitations (Eelman et al., 2008; Lubben et al., 2008). High energy ionization conditions such as those in in electron impact sources induce fragmentation of the analytes making structure determination difficult. Alternatively, lower energy or soft ionization techniques, such as ESI and Matrix Assisted Laser Desorption Ionization (MALDI), have been successfully used for soluble, ionic compounds. However, these are not useful for compounds that are insoluble in the matrices required for these soft techniques (Eelman et al., 2008). In the case of ESI, even some of the analytes that are soluble are not detectable by mass spectrometry as they exist as neutrals in solution making derivatization necessary prior to analysis by mass spectrometry (Lubben et al., 2008). Eelman suggested that direct analysis of solid samples would be very desirable (Eelman et al., 2008). We hypothesize that if an appropriate delivery system can be developed to produce solvent free vapour of synthetic products that photoionization could be an effective way to produce molecular ions.

1.8 Ambient ionization

The term ambient ionization is currently used to describe a series of mass spectrometric ionization techniques where samples are analyzed "neat" with little or no sample preparation or separation by forming ions outside the mass spectrometer and drawing characteristic ions into the mass spectrometer for analysis (Venter et al., 2008). This approach has been proven to be useful for the analysis of many important classes of compounds, for example drugs of abuse, explosives and chemical warfare agents. Ambient ionization generally operates at atmospheric pressure, in open air and offers soft ionization of a sample in its native state (Cody et al., 2005; Venter et al., 2008).

The recent interest in ambient ionization was initiated by the announcement of desorption electrospray ionization (DESI) in 2004 (Venter et al., 2008). Using an electrospray plume to desorb and ionize samples dried onto a movable stage, DESI produces ESI like mass spectra (Takáts et al., 2004). A new field of DESI-like techniques has developed for the rapid analysis of a variety of analytes (Venter et al., 2008). An improvement on the DESI technique was the development of discharge based sources with the introduction of direct analysis in real time (DART) (Cody et al., 2005). The technique uses a helium discharge at atmospheric pressure to produce a metastable atom bombardment source that can ionize a wide range of analytes (Cody et al., 2005). The precise mechanism of DART has not been settled but is often attributed to helium metastables or nitrogen cations making it very similar to Penning ionization (ionization via rare gas metastable molecules) that has been has been examined for mass spectrometric applications since the 1970's (Cody et al., 2005; Jones and

Harrison, 1971). Another ambient technique, Atmospheric pressure Solids Analysis Probe (ASAP), uses a glass rod dipped into a sample solution and placed in a traditional atmospheric pressure source where the sample is heated by the by the typical desolation gases and ionized by APCI (McEwen et al., 2005). Several versions of low temperature discharge (LTD) plasmas have been developed for ambient desorption ionization that use an electrical discharge across a dielectric barrier generating a plasma that desorbs and ionizes surface molecules (Andrade et al., 2006; Harper et al., 2008).

Ionization of headspace vapours is related to ambient ionization. In a comparison of spectra of polycyclic aromatic hydrocarbons (PAHs) dissolved in solvents to the spectra of the headspace vapours above pure crystals of the same PAHs, Syage et al. found that the spectra of solventless PAHs contained M^+ while the spectra of PAH solutions had $[M+H]^+$ as the dominant ion (Syage 2004). A KrF laser pulse has been used to desorb and ionize nucleic acids and PAHs producing predominately molecular ions has been described (Antonov et al., 1980). Desorption photoionization via a nebulizer system that delivered a heated jet of vaporized solvent to desorb surface molecules prior to photo ionization by a standard krypton lamp was developed (Haapala et al., 2007) and it has been found that PAHs with more than four rings may require additional effort to vapourize prompting development of a heated nozzle useful in studies of Penning ionization (Yamakita et al., 2009). Given this, it is clear that additional approaches using APPI would be consistent with current trends and directions.

1.9 Hypothesis

This thesis seeks to address two distinct but related hypotheses. Our first hypothesis is that photoionization is independent of discharge gas used. In order to test this hypothesis, a custom made photoionization lamp was constructed that enabled the discharge gas to be conveniently changed. Our second hypothesis is that vapours of aromatic hydrocarbons and organometallic compounds will be ionized by Atmospheric Pressure Photoionization yielding molecular ions and structural information.

Chapter 2: Experimental

2.1 Introduction

In this chapter we will outline the experimental parameters and techniques that were used to test the hypothesis outlined in section 1.9. In section 2.2 we outline the experimental set up to demonstrate that photoionization is independent of gas type used. In section 2.3 we outline the experimental set up to demonstrate that Atmosphere Pressure Photoionization is a valuable way to characterize vapours of synthetic products and byproducts.

2.2 Lightning Ion Source

We have developed a unique photoionization lamp and ionization source called the Lightning Ion Source (LIS) to generate photons from a series of gas types. Figure 2 is a schematic diagram of the LIS. One of the main considerations for engineering was the ease of incorporation onto the Waters Quattro Premier LC-MS/MS taking into account the geometry and space restrictions of the aluminum source block. Additionally, there could no arcing of current between the new source and the source enclosure.

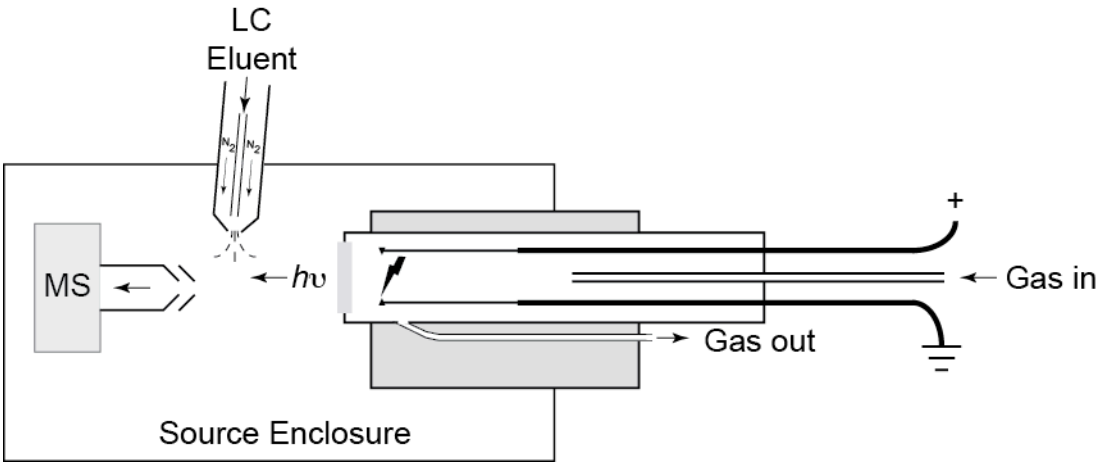

Figure 2: Schematic of Emco powered Lightning Ion Source

The existing krypton lamp assembly was removed from the back of the enclosure revealing a 34 mm by 39 mm oval hole. The discharge chamber was manufactured from a 13 mm diameter poly tetrafluorinated ethylene (PTFE) rod that was hollowed out leaving a 9.2 mm interior diameter. Two 1.5 mm holes were drilled in the back to allow for electrodes to be inserted. Various electrode materials were evaluated. It was found that copper, steel and stainless steel electrodes disintegrated in the high voltage discharge conditions. Tungsten welding rods were found to give most steady and intense discharge without appreciable wearing of the electrodes after prolonged use. The orientation and shape of the electrodes were optimized to avoid premature arching midway down the electrodes. The electrodes were ground down to 50% thickness (0.75 mm) for the last inch ending in a full diameter tip

The end of the PTFE chamber was fitted with a lithium fluoride window 3 mm in thickness and 10 mm in diameter. Using a tap and die set, the inside diameter of the PTFE rod was threaded so the window could be screwed into the rod and partially sealed with PTFE tape. The window was intermittently polished with an aluminum oxide slurry on a polishing plate

or wiped with a methanol doused tissue. The portion of the tungsten electrodes outside the Teflon™ discharge chamber were encased in several layers of polyolefin heat shrink tubing (Princess Auto SKU 8292435) to prevent unintended arcing out the back. Two gas lines were incorporated into the top and bottom of the teflon discharge tube to deliver various gases and remove the excess gas. The outflow tube was vented into the lab air maintaining a pressure close to atmospheric in the chamber. The gases were delivered by PTFE tubes connected by brass fittings. Connections between the DC/DC converter and electrodes were made via alligator clips with additional electrical shielding. The input to the Emco DC/DC high voltage converter was a HY1303D power supply at 13 V and 0.46 amps.

2.2.1 Instrumentation

2.2.1.1 Mass spectrometer

All mass spectra were generated on a Waters Quattro Premier triple quadrupole mass spectrometer. The operating conditions are given in Table 1. For comparison between the commercial lamp and the lab built versions the instrument parameters were optimized for each compound with the APPI lamp and those conditions were used for the LIS with the exception of the repeller voltage (as a repeller electrode was not present).

Table 1: Lightning Ion Source mass spectrometer conditions

Parameter	Setting	Parameter	Setting
Repeller Voltage	0	Source Temperature	150°C
Cone Voltage	20 volts	Desolvation Temperature	400°C
Extractor	7 volts	Desolvation gas flow	450 l/hr
RF Lens	1.0	Cone Gas	40 l/hr
Low Mass Resolution 1	15	Low Mass Resolution 2	15
High Mass Resolution 1	15	High Mass Resolution 2	15
Ion Energy 1	1.0	Ion Energy 2	2.0
Entrance	24		
Collision	2	Multiplier	650
Exit	24		

2.2.1.2 Optical spectrometer

Photon emission spectra were collected using an Ocean Optics LIBS 2000+ fibre optic spectrometer. Emission spectra of the lab made ion source with various gases were measured as well as the commercial low pressure krypton lamp. The Waters PhotoMate™ lamp was removed from the back of the source and the fiber optic probe placed directly in front of the lamp. The room lights were turned off and black cloth placed over the setup to limit light

contamination. A spectral reading verified that the background light was zero before measurements were taken. The NIST spectral database was queried for reference photo emission lines.

2.2.1.3 Liquid chromatography

Using the standard configuration on the Waters system, methanol solvent was pumped using a Waters HPLC pump operating at 0.200 ml min^{-1} through a Waters C_{18} guard column to the APPI probe head at a pressure of 200 kPa.

2.2.2 Chemicals and discharge gases

Naphthalene, 17-α-hydroxyprogesterone, pyrene and anthracene authenticated standards of 97% purity or higher were obtained from Sigma Aldrich (Mississauga, ON). Nitrogen, argon, hydrogen, oxygen, carbon dioxide, helium at 99.999% from (Air Liquide) and compressed air were all examined as discharge gases.

2.2.3 Standard solutions

A series of solutions (4 to 75 ug/ml) containing pyrene, anthracene, naphthalene and 17-α-hydroxyprogesterone were prepared from pure crystals in volumetric glassware in methanol (HPLC Grade; Fischer Scientific Inc., Mississauga, ON). All glassware was cleaned with de-ionized water, rinsed twice with HPLC methanol and dried at 100°C. To ensure full dissolution the initial stock solution was sonicated for 15 minutes, and allowed to cool to

room temperature for 20 minutes prior to serial dilution. Standard solutions were either injected manually into the 5 μL sample loop via a 100 μL syringe or automatically sampled from vials within a Waters Alliance 2695 system. Mass spectra for each compound were collected in triplicate injections with each of the discharge gases and compared to the commercial krypton lamp. To examine sensitivity, naphthalene solutions were ionized by various discharge gases and compared to the commercial krypton lamp. Linear regression and ANOVA analysis were carried out using Prism statistical software version 5.0.

2.3 Using atmospheric pressure photoionization to characterize vapours

To determine whether vapour introduction would allow for rapid analyte characterization and identification a sample introduction apparatus was built. The design of the Thermally Assisted Vapour Introduction (TAVI) apparatus had to be incorporated into the Waters Quattro Premier LC-MS/MS with its inherent geometry and the space restrictions of the aluminum source block. As with the Lightning Ion Source, there could no arcing of current between the new source and the source enclosure, APPI probe head or especially the cone and subsequent mass spectrometer.

The TAVI apparatus was built from a new modified Iron Fist adjustable 60 W soldering iron (Princess Auto SKU 8103590) that was used as a heating element. The steel sheath of the soldering iron was removed leaving the heating wiring and electrical connections. An aluminum holder was constructed to allow positioning of the end of the sample tube directly under the photoionization lamp. A ceramic collar was fabricated to fit the soldering iron's heating tube and attach the heating tube to the aluminum holder. The heating element was

held in place to the ceramic collar by a lock nut. The aluminum holder was attached to the main door of the source using the existing screws of the door. Temperature of the heating apparatus was controlled by the original soldering iron heat dial that was calibrated against a thermocouple. A Powerfist DT-838 thermocouple temperature gauge was placed next to the capillary tube holder in the heating tube to measure the temperature. A copper insert was manufactured and threaded into the end of the heating tube and sealed with ceramic cement. The heating tube was positioned as close to the repeller plate as possible without arcing from the repeller to the heating element. A few milligrams of each analyte was placed into standard glass capillary tubes that were cut to 11 mm. The sample tubes were inserted into the heater.

With the commercial Syagen photoionization source and probe head assembly in place, the standard front window of the source block was removed and the TAVI apparatus inserted through the front.

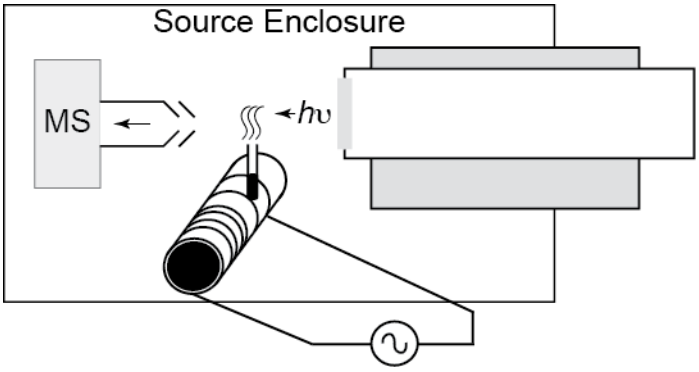

Figure 3: TAVI apparatus

2.3.1 Instrumentation

The instrument was optimized for naphthalene and the same conditions were used for subsequent compounds (Table 2). In addition to MS measurements, MS/MS collision induced dissociation (CID) experiments were conducted to fragment the analytes and identify compounds.

Table 2: TAVI source mass spectrometer conditions

Parameter	Setting	Parameter	Setting
Repeller Voltage	2.0 kV	Source Temperature	150°C
Cone Voltage	24 volts	Desolvation Temperature	150°C
Extractor	4 volts	Desolvation gas flow	0 L/hr
RF Lens	1.6	Cone Gas	0 L/hr
Low Mass Resolution 1	12	Low Mass Resolution 2	12
High Mass Resolution 1	12	High Mass Resolution 2	12
Ion Energy 1	1.0	Ion Energy 2	2.0
Entrance	24		
Collision	2	Multiplier	650
Exit	24		

2.3.2 Chemicals

Naphthalene, trans stilbene, 17-α-hydroxyprogesterone, biphenyl, rescorinol, flavanone, stilbene, 2,4-dinitrophenol, pyrene, anthracene, benzdiamine, ferrocene, decafluorobiphenyl, Phenanthrene, ethyl-4-aminobenzoate and fluoroanthene were purchased from Sigma Aldrich Canada (Mississauga, ON). Salicylic acid was obtained from BDH chemicals (Fisher Scientific, Mississauga, ON). 9-methylanthracene was obtained from Avocado research Chemical Limited (Alfa Aesar, Ward Hill, MA).

$Cr(acac)_3$ was prepared by combining 5 mmol chromium(III) chloride, 167 mmol urea and 30 mmol acetylacetone. The mixture was heated to 90°C for 90 minutes and deep maroon crystals were collected.

$Fe(acac)_3$ was prepared by combining 12 mmol of iron(III) chloride hexahydrate, 38 mmol of acetylacetone in methanol and 62 mmol of sodium acetate and heated to 80°C for 15 minutes. The solution was ice-cooled and red precipitate collected.

Novel compounds (LG113, LG159) were synthesized as previously described as part of a pharmacology project on tumor cells lines (Gurley et al., 2011). The molecular weight of LG113 and LG159 are 353.3 and 316.4 grams respectively.

Chapter 3: Results

3.1 Lightning Ion Source

Data was collected to describe 3 aspects of the LIS: (1) characterization of the emission spectra, (2) comparisons between mass spectra from the krypton lamp and the LIS and (3) a comparison of calibration curves for quantification.

3.1.1 Emission spectra

The emission spectra of argon, hydrogen, helium, oxygen and nitrogen were measured and compared to NIST reference lines to ensure that the LIS was producing photons indicative of the discharge gas (Tables 3-7). Three replicate measurements of the emission spectra of carbon dioxide and the commercial krypton lamp were found to be reproducible with an average relative standard deviation of 3% of peak intensity between the runs.

Table 3 shows a comparison of argon emission lines generated by the LIS and the NIST expected values. There is an average of 0.02% variation of the wavelengths. For comparison, Table 3 gives reference and experimental intensities relative to 763.51 nm emission line. There is an average of 3800% difference between the NIST reference intensities and the measured intensities with the greatest deviation at the 337.347 nm wavelength.

Table 3: Comparison of the predicted NIST reference emission profile of argon to experimental values.

NIST Wavelength (nm)	Intensity	Relative Intensity	Experimental Wavelength Range (nm)	Experimental Average Wavelength (nm)	Intensity	Relative Intensity	% Deviation from Expected Wavelength	% Deviation from Expected Intensity
337.3470	7	0.03	336.8-337.4	337.1	12.	17.4	0.07	62,000
357.6616	70	0.28	357.4-357.8	357.6	12.	17.8	0.02	6,200
372.9309	70	0.28	372.7-373.1	372.9	9.	13.5	0.01	4,700
380.3172	25	0.10	380.2-380.5	380.4	8.	12.5	0.02	13,000
385.0581	70	0.28	384.8-385.1	385.0	8.	12.2	0.02	4,200
434.8064	800	3.22	434.2-435.3	434.8	14.	21.1	0.00	550
437.9667	150	0.60	437.7-438.1	437.9	9.	13.8	0.02	2,200
440.0986	200	0.84	439.9-440.4	440.2	9.	14.1	0.02	1,600
442.6001	400	1.54	441.8-443.4	442.6	12.	17.4	0.00	1,000
454.5052	400	1.54	454.2-454.8	454.5	9.	13.8	0.00	800
457.9350	400	1.60	457.6-458.2	457.9	9.	14.1	0.01	790
458.9898	400	1.60	458.6-459.4	459.0	11.	15.8	0.00	890
460.9567	550	2.20	460.4-461.5	461.0	12.	18.1	0.01	720
465.7901	400	1.60	465.4-466.0	465.7	10.	14.5	0.02	810
472.6868	550	2.20	472.2-473.0	472.6	10.	15.1	0.02	590
473.5906	300	1.20	473.0-473.9	473.5	11.	16.4	0.02	1,300
476.4865	800	3.21	476.0-476.9	476.5	10.	15.1	0.00	370
480.6020	550	2.20	480.0-481.1	480.6	14.	20.7	0.00	840
484.7810	150	0.60	484.2-485.1	484.7	10	15.1	0.02	2,400
487.9864	800	3.21	487.25-488.5	487.9	12.	17.4	0.02	440
493.3209	35	0.14	492.8-493.5	493.2	9.	12.8	0.02	9,100
514.1783	100	0.41	513.7-514.6	514.2	14.	20.4	0.00	4,900
696.5543	10,000	40.00	696.2-696.9	696.6	23.	35.2	0.01	12
706.7218	10,000	40.00	706.2-707.6	706.9	21.	31.6	0.03	21
727.2936	2000	7.99	727.1-727.7	727.4	11.	15.8	0.01	100
738.3980	10,000	40.00	738.2-738.9	738.6	33.	49.7	0.03	24
742.5294	10	0.04	742.3-742.7	742.5	11.	16.4	0.00	39,000
750.3869	20,000	79.99	750.1-751.1	750.6	27.	40.1	0.03	50
751.4652	15,000	60.00	751.2-752.1	751.7	32.	48.0	0.03	20
763.5106	25,000	100.00	762.8-765.2	764.0	66.	100.0	0.06	-
772.3761	15,000	60.00	772.1-773.0	772.6	24.	36.5	0.03	39
794.8176	20,000	79.99	796.6-795.5	795.1	18.	27.6	0.04	65
800.6157	20,000	79.99	800.5-801.0	800.8	27.	40.8	0.02	49
801.4786	25,000	100.00	801.0-802.2	801.6	50.	76.0	0.02	24
810.3693	20,000	79.99	809.6-810.8	810.2	81.	122.0	0.02	52
811.5311	35,000	140.00	811-812.6	811.8	218.	328.9	0.03	130
826.4522	10,000	40.00	826.0-827.0	826.5	42.	63.8	0.01	60
840.8210	15,000	60.00	840.3-841.6	841.0	83	125.0	0.02	110
842.4648	20,000	79.99	841.6-843.3	842.5	100	150.7	0.00	90
852.1442	15,000	60.00	851.8-852.5	852.2	36.	54.3	0.01	10
912.2967	35,000	140.00	912.0-912.9	912.5	28.	41.8	0.02	70
922.4499	15,000	60.00	922.1-923.4	922.8	13.	19.1	0.04	70

Table 4 shows a comparison of hydrogen emission lines and the NIST expected values. There is an average of 0.06% variation between the reference wavelengths and the measured experimental wavelengths. There is an 84% difference between the NIST reference intensity values and the measured intensity values.

Table 4: Comparison of the predicted NIST reference emission profile of hydrogen to experimental values.

NIST Wavelength (nm)	Intensity	Relative Intensity	Experimental Range (nm)	Experimental Average Wavelength (nm)	Intensity	Relative Intensity	% Deviation from Expected Wavelength	% Deviation Intensity
486.1330	80	44.	476.0-495.5	485.8	200	6.7	0.07	85
656.2852	180	-	650.0-663.1	656.6	3,000	-	0.05	-

Table 5 shows a comparison of helium emission lines and the NIST expected values. There is an average of 0.11% variation between the reference wavelengths and the measured wavelengths. For comparison, Table 5 also gives intensities relative to 587.60 nm emission line for each of the reference and experimental emission peaks. There is an average of 1600% difference between the NIST reference intensities and the measured intensities with the greatest deviation at the 906.327 nm wavelength.

Table 5: Comparison of the predicted NIST reference emission profile of helium to experimental values.

NIST Wavelength (nm)	Intensity	Relative Intensity	Experimental Range (nm)	Experimental Average Wavelength (nm)	Intensity	Relative Intensity	% Deviation from Expected Wavelength	% Deviation Intensity
370.5000	3	.6	370.3-371.2	370.8	125	15.0	0.08	2,400
587.5970	500	100	580.7-591.0	585.9	833	100	0.29	-
655.0100	8	1.6	653.6-658.2	655.9	177	21.2	0.14	1,200
667.0100	100	20	664.9-670.8	667.9	172	20.6	0.01	3.2
706.5190	200	40	705.4-709.8	707.6	151	18.1	0.15	55.
906.3270	2	0.4	905.7-907.0	906.4	152	18.2	0.01	4,400

Table 6 shows a comparison of oxygen emission lines and the NIST expected values. There is an average of 0.16% variation from the reference wavelengths and the measured wavelengths. For comparison, Table 6 also gives intensities relative to the 777.417 nm emission line. There is an average of 1800% difference between the NIST reference intensities and the measured intensities with the greatest deviation at the 868.609 nm wavelength.

Table 6: Comparison of the predicted NIST reference emission profile of oxygen to experimental values.

NIST Wavelength (nm)	Intensity	Relative Intensity	Experimental Range (nm)	Experimental Average Wavelength (nm)	Intensity	Relative Intensity	% Deviation from Expected Wavelength	% Intensity
244.5538	22	2.7	244.3-244.9	244.6	153	23.4	0.019	760
278.3026	6	0.7	278.33	278.3	177	27.0	0.010	3548
298.3780	250	31.	298.3-298.5	298.4	154	23.5	0.007	24
326.0980	200	25.	325.8-326.2	326.0	136	20.8	0.030	16
326.5460	300	37.	326.3-328.1	326.7	146	22.3	0.047	40
372.7320	27	3.3	372.5-373.1	372.8	166	25.3	0.018	660
374.9486	30	3.7	374.8-375.2	375.0	196	29.9	0.014	708
388.2446	13	1.6	388.0-388.8	388.4	170	26.0	0.040	1517
391.1957	20	2.5	391.1-391.6	391.4	171	26.1	0.052	957
391.9285	18	2.2	391.6-392.3	391.9	175	26.7	0.007	1102
395.4362	20	2.5	395.2-395.8	395.5	184	28.1	0.016	1038
397.3257	24	3.0	396.9-397.8	397.3	230	35.1	0.006	1085
407.2157	23	2.8	406.2-408.3	407.1	502	76.6	0.028	2599
412.0280	17	2.1	411.6-412.7	412.1	348	53.1	0.017	2431
414.5699	6	0.7	413.9-415.0	414.4	228	34.8	0.041	4599
415.3298	18	2.2	415.0-415.8	415.4	230	35.1	0.017	1480
418.9789	20	2.5	418.1-419.6	418.9	284	43.4	0.019	1656
431.7700	11	1.4	431.4-432.3	431.8	237	36.2	0.007	2564
434.9426	23	2.8	434.1-435.7	434.9	386	58.9	0.010	1975
441.4905	27	3.3	440.8-442.4	441.6	365	55.7	0.025	1572
444.7673	5	0.6	444.2-445.4	444.8	245	37.4	0.007	5960
459.5960	7	0.9	458.4-460.4	459.4	359	54.8	0.043	6242
464.1810	22	2.7	463.6-465.7	464.7	646	98.6	0.112	3531
466.1633	21	2.6	465.7-466.5	466.1	284	43.4	0.014	1572
467.6235	20	2.5	467.8-468.2	468.0	261	39.8	0.081	1514
470.3163	14	1.7	468.7-472.1	470.9	380	58.0	0.124	3257
490.6833	19	2.3	490.3-491.2	490.7	171	26.1	0.003	1013
492.4531	21	2.6	491.9-492.9	492.4	186	28.4	0.011	995
494.2999	20	2.5	493.3-494.9	494.1	212	32.4	0.040	1211
517.5896	12	1.5	516.6-518.5	517.5	234	35.7	0.017	2311
648.3979	12	1.5	647.4-648.5	648.0	233	35.6	0.061	2301
655.0598	4	0.5	654.9-657.3	656.1	229	35.0	0.159	6980
660.4910	80	9.9	660.1-661.4	660.7	221	33.7	0.032	242
715.6090	11	1.4	714.9-716.5	715.7	217	33.1	0.013	2340
777.4170	810	100	775.0-780.1	777.6	655	100.0	0.024	0
795.0800	210	26	794.3-795.6	755.0	159	24.3	5.041	6
822.1820	400	49	820.6-823.9	822.3	335	51.1	0.014	4
844.625	810	100	842.3-847.7	845.0	629	96.0	0.044	4
868.6088	8	1.	867.5-869.5	868.5	347	53.0	0.013	5264
882.0430	325	40.	881.4-882.8	882.1	167	25.5	0.006	36
926.5940	490	61.	924.7-930.7	927.7	271	41.4	0.119	32

Table 7 shows a comparison of nitrogen emission lines and the NIST expected values. There is an average of 0.03% variation from the reference wavelengths and the measured wavelengths. For comparison, Table 7 also gives intensities relative to 821.63 nm emission line. There is an average of 47% difference between the NIST reference intensities and the measured intensities with the greatest deviation at the 460.63 nm wavelength.

Table 7: Comparison of the predicted NIST reference emission profile of nitrogen to experimental values.

NIST Wavelength (nm)	Intensity	Relative Intensity	Experimental Range (nm)	Experimental Average Wavelength (nm)	Intensity	Relative Intensity	% Deviation from Expected Wavelength	% Intensity
343.715	360	63	343.6-344.3	344	142	32	0.08	49.2
391.9	360	63	391.0-392.6	391.8	137	31	0.03	51.0
393.852	90	16	392.7-394.7	393.7	137	31	0.04	95.9
399.5	1000	175	398.6-400.5	399.6	252	57	0.03	67.6
403.508	360	63	401.9-405.6	403.8	178	40	0.07	36.4
409.733	250	44	409.1-410.8	409.9	167	38	0.04	14.0
423.691	285	50	422.5-424.8	423.7	162	37	0.00	26.9
444.703	650	114	444.0-445.2	444.6	200	45	0.02	60.4
460.148	550	96	460.0-460.5	460.3	195	44	0.03	54.4
460.633	90	16	460.6-461.0	460.8	189	43	0.04	170.2
461.387	360	63	461.2-461.6	461.4	174	39	0.00	37.8
462.139	450	79	461.9-462.4	462.2	192	43	0.01	45.1
463.054	870	153	462.7-463.6	463.1	329	74	0.01	51.3
464.308	550	96	463.9-464.6	464.3	218	49	0.00	49.0
478.813	285	50	478.6-479.2	478.8	150	34	0.00	32.3
480.329	450	79	479.9-480.9	480.4	167	38	0.01	52.2
500.515	870	153	498.4-502.4	500.4	350	79	0.02	48.2
504.51	550	96	504.2-505.1	504.7	146	33	0.04	65.8
553.536	285	50	552.0-554.6	553.3	172	39	0.04	22.3
566.663	650	114	565.9-567.6	567.3	227	51	0.11	55.1
567.956	870	153	567.1-568.7	567.9	325	73	0.01	51.9
571.024	450	79	570.6-571.8	571.2	156	35	0.03	55.4
594.024	285	50	593.6-594.6	594.1	166	37	0.01	25.1
648.171	265	46	647.3-648.9	648.1	179	40	0.01	13.1
661.056	750	132	659.7-661.6	660.7	178	40	0.05	69.5
744.229	785	138	744.1-744.7	744.4	170	38	0.02	72.1
818.802	400	70	818.1-819.4	818.8	277	63	0.00	10.9
821.634	570	100	821.4-822.1	821.8	443	100	0.02	0.0
822.314	400	70	822.1-822.6	822.4	273	62	0.01	12.2
824.239	400	70	823.8-824.8	824.3	246	56	0.01	20.9
859.4	570	100	858.9-860.3	859.6	170	38	0.02	61.6
862.924	650	114	862.5-863.9	863.2	231	52	0.03	54.3
865.589	500	88	865.3-866.3	865.8	157	35	0.02	59.6
868.34	650	114	867.2-869.7	868.5	495	112	0.02	2.0
870.325	500	88	870.1-870.8	870.5	210	47	0.02	46.0
939.279	570	100	938.9-939.7	939.3	150	34	0.00	66.1

3.1.2 Mass spectra generated with Lightning Ion Source

The mass spectra of pyrene generated by the lab built LIS and the commercial krypton lamp was dominated by molecular cation as seen in Figure 4. The average levels of $[M]^+$, $[M+H]^+$ and $[M+2\ amu]^+$ for two replicate runs are given in Table 8. It is noteworthy that the Lightening Ion Source (LIS) gave up to a 88% stronger signal for the molecular peak compared to the same concentration used with the commercial krypton lamp as given in Table 8. The isotope ratio produced by the argon LIS was closer to the expected values of 17.5% and 1.4% than the commercial krypton source.

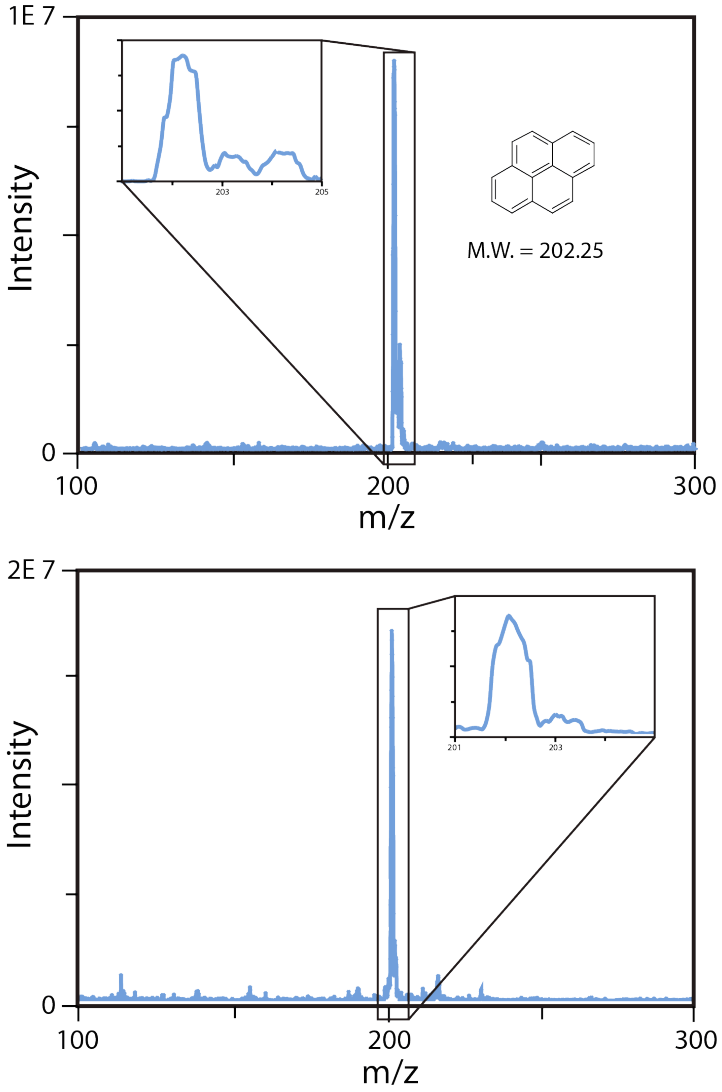

Figure 4: Mass spectra of pyrene by commercial kr (top) and the LIS (bottom)

Table 8: Comparison of peak area of duplicate pyrene signals from the commercial lamp and argon lab made Lightning Ion Source

m/z	Average of Peak Height of Pyrene		
	APPI Krypton Lamp	**Argon Lightning Ion Source**	**Percent Signal Increase of LIS**
202.1	8.94×10^6	1.68×10^7	88%
203.1	1.74×10^6 (19.4%)	2.73×10^6 (16.3%)	57%
204.1	1.96×10^6 (21.9%)	3.98×10^5 (2.4%)	- 80%

17-α-hydroxyprogesterone was ionized by the LIS and revealed the usual $[M+H]^+$ parent peak associated with photoinduced chemical ionization shown in Figure 5. The LIS gave approximately eight times the signal for the same sample as shown in Table 9. In addition to $[M+H]^+$ peak, the commercial krypton lamp gave other peaks at $[M+H]^+ + 32$ and + 53 amu that were not seen to the same extent on the spectra generated by the LIS. The isotope ratio produced by the argon LIS was closer to the expected values of 23.3% and 3.2% than the commercial krypton source.

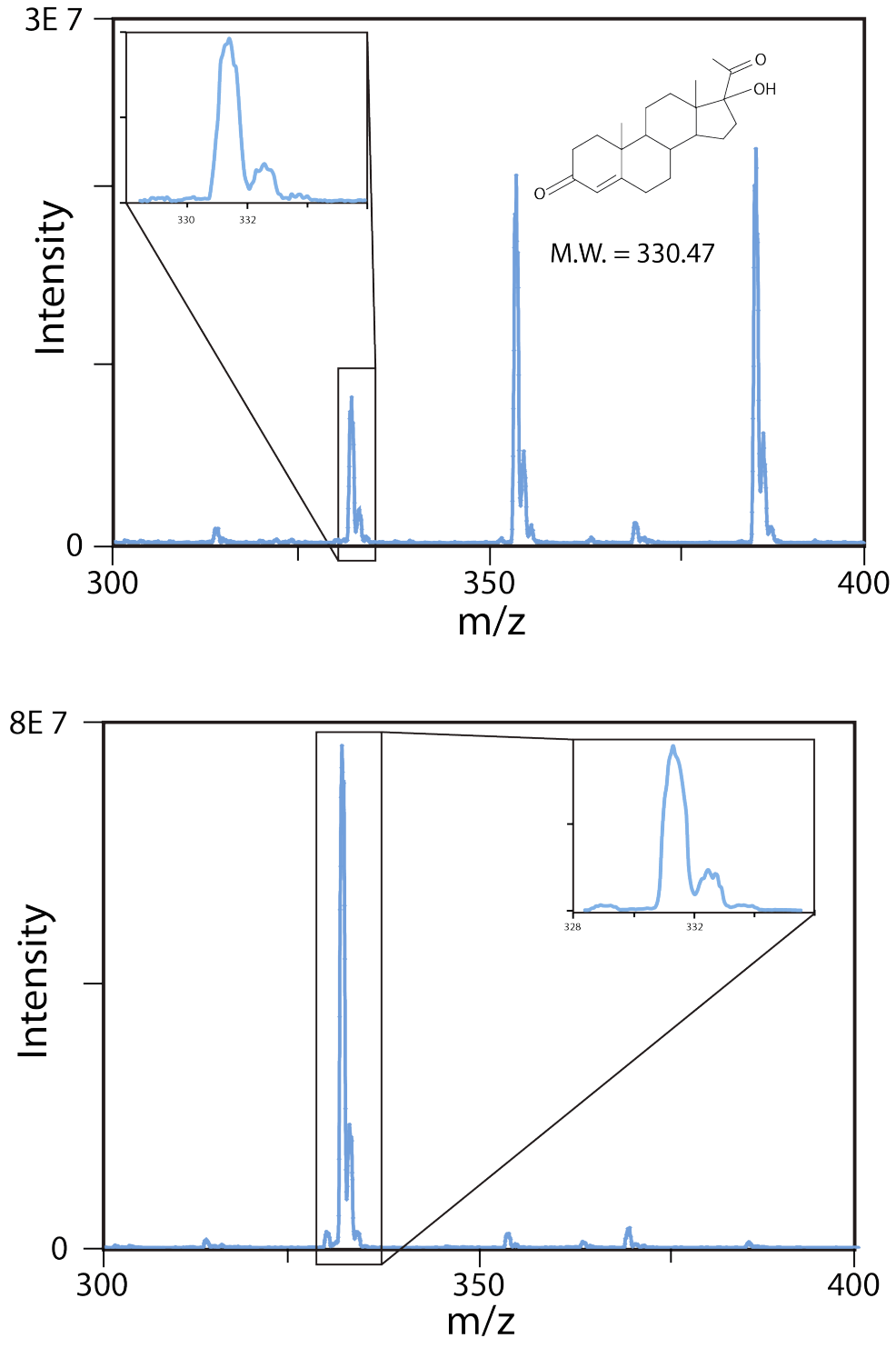

Figure 5: Mass spectra of 17-α-hydroxyprogesterone by commercial kr (top) and the LIS (bottom)

Table 9: Comparison of duplicate measurements of peak height of commercial lamp and argon LIS for 17-α-hydroxyprogresterone

m/z	Average of Peak Height of 17-α-hydroxyprogesterone		
	APPI Krypton Lamp	**Lab Made Argon Lightning**	**Percent Signal Increase of LIS**
331.5	8.24×10^6	7.61×10^7	820%
332.5	1.88×10^6 (22.8%)	1.87×10^7 (24.6%)	890%
333.5	3.27×10^5 (4.0%)	2.39×10^6 (3.1%)	630%
353.5	2.08×10^7	2.11×10^6	- 90%
354.5	5.19×10^6	4.70×10^5	-90
355.5	6.35×10^5	9.60×10^4	- 85%
385.5	2.23×10^7	8.29×10^5	-63%
386.5	6.22×10^6	1.87×10^5	- 97%
387.5	9.22×10^5	1.30×10^5	-86%

3.1.3 Calibration curves

To determine whether the discharge gases tested produced linear responses with increasing analyte concentration a series of calibration curves were constructed. From the replicate measurements the percent relative standard deviation and linear regression was calculated. Using a linear relation between peak area and analyte concentration a correlation coefficient was determined. The validity of a linear fit was examined through examination of the residuals from the linear model.

For all the gases tested with naphthalene, the LIS was more sensitive as measured by increased response factors compared to the commercial krypton source. Limits of detection, defined as 3 times the standard deviation of the instrumental noise, varied on the LIS but were found to not be as low as the commercial krypton source with the exception of oxygen

that was found to be lower than the commercial krypton lamp. Table 10 summarizes the figures of merit. The detection limit of the commercial krypton source was lower than all of the other gases. This could be due to the nature of the photon flux generated by the lamp or perhaps due to the repeller plate that is mounted around the lithium fluoride window that was not part of the LIS. The repeller plate supplies a repelling voltage to help direct ion towards the cone and orifice. Interestingly, the sensitivity of the LIS, as measured by the slope of the line of best fit, was much greater than the commercial lamp. The increase in sensitivity could be due to the increased current used by the LIS generating a greater photon flux.

Table 10: Comparison of figures of merit of discharge gas using naphthalene

Discharge gas	Lowest Detection level (ug/ml)	Slope of linear regression line	Average % RSD of replicates	Correlation
Kr (Commercial)	0.312	696,000	7%	0.9982
Air (LIS)	1.97	3,610,000	8%	0.9826
He (LIS)	0.624	4,110,000	4%	0.9936
N_2 (LIS)	0.984	4,270,000	8%	0.9968
Ar (LIS)	1.97	4,270,000	7%	0.9943
H_2 (LIS)	0.984	4,600,000	15%	0.9760
O_2 (LIS)	0.078	4,070,000	16%	0.9874
CO_2 (LIS)	0.984	4,820,000	4%	0.9945

3.1.3.1 Krypton discharge lamp

The results of the evaluation of the commercial krypton discharge lamp is given in Table 11. The commercial krypton discharge lamp had a limit of quantification less than 0.312 ug/ml. Peak area response was found to be linear from 0.312 ug/ml to 73.9 ug/ml with a correlation coefficient of 0.9982. The average percent relative standard deviation was 7% between the three replicate samples. The linear relation is defined by peak area = (696,000+/- 6,000) x [Naph Conc.] - (500,000 +/- 300,000). An analytical calibration curve of peak area to concentration is given in Figure 6. The residual analysis in Figure 7 supports the linear relation between concentration and peak area for the commercial lamp.

Table 11: Peak area as a function of naphthalene concentration

[Naphthalene] (ug/ml)	**Peak Area**			**% RSD**
	1	**2**	**3**	
0.312	210,913	178,415	181,409	9
0.624	531,333	550,500	499,568	14
0.984	505,403	568,689	534,133	6
1.97	1,287,752	1,109,774	1,152,917	10
3.94	2,433,902	2,514,515	2,476,247	2
24.6	16,831,232	17,359,430	17,323,798	3
49.3	32,306,436	35,131,560	33,661,750	4
73.9	50,632,636	49,299,932	51,106,128	4

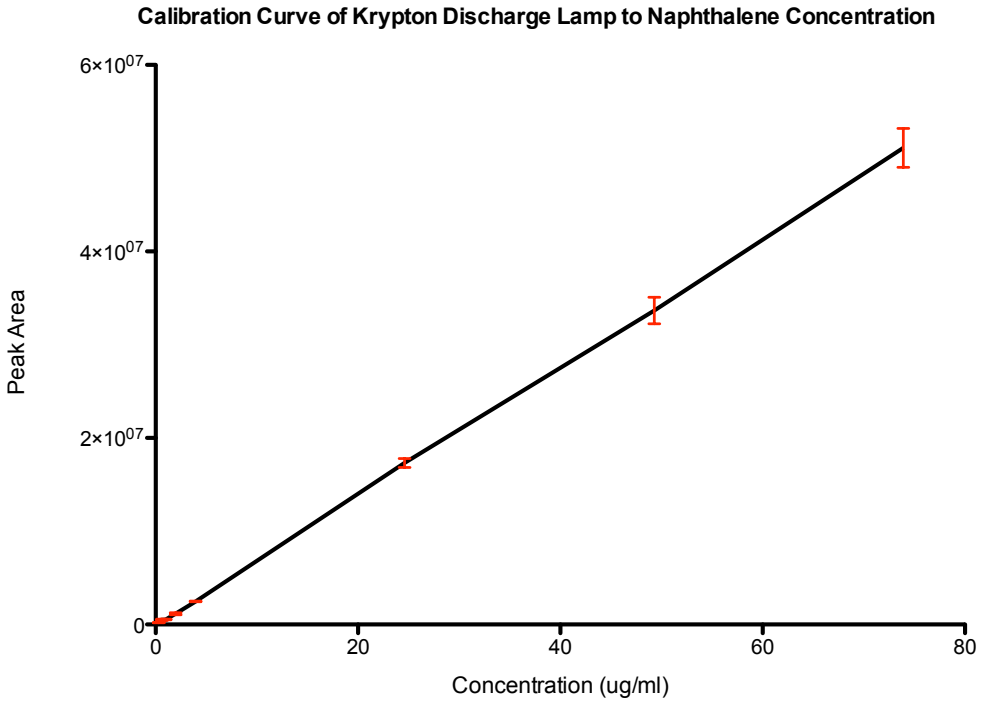

Figure 6: Analytical calibration curve of naphthalene to krypton discharge

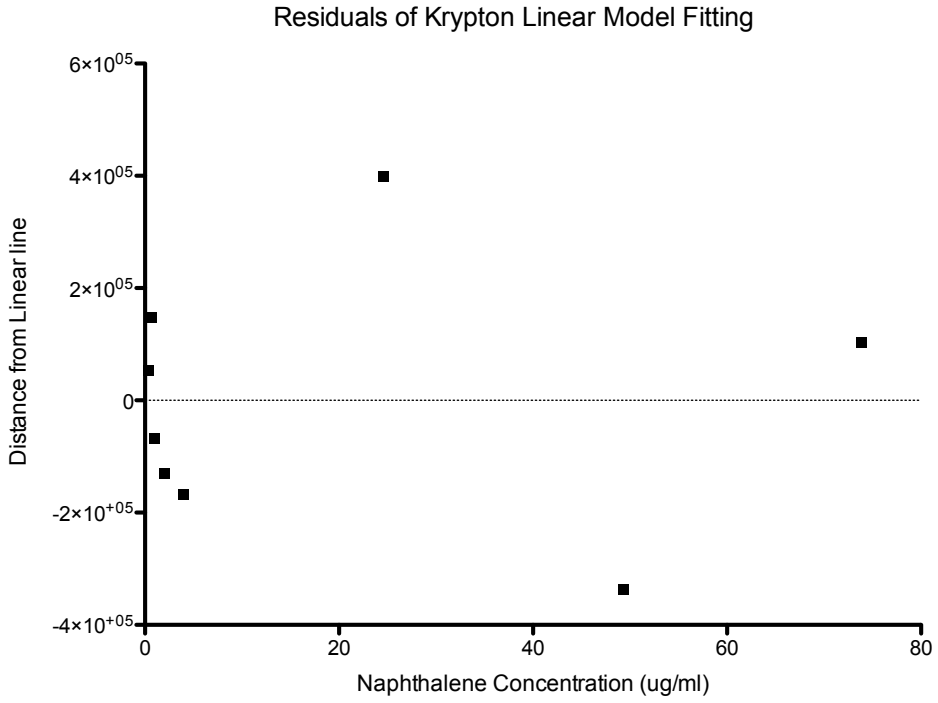

Figure 7: Residuals of naphthalene linear regression for krypton discharge

3.1.3.2 Air discharge lamp

The results of the evaluation of the air discharge lamp is given in Table 12. The air discharge lamp had a limit of quantification less than 1.97 ug/ml. Peak area response was found to be linear from 1.97 ug/ml to 73.9 ug/ml with a correlation coefficient of 0.9826. The average percent relative standard deviation was 8% between the three replicate samples. The linear relation is defined by Peak Area = (3,610,000+/- 70,000) x [Naph Conc.] - (3,000,000 +/- 3,000,0000). An analytical calibration curve of peak area to concentration is given in Figure 8. The residual analysis in Figure 9 supports the linear relation between concentration and peak area for the air discharge LIS.

Table 12: Peak area as a function of naphthalene concentration

[Naphthalene] (ug/ml)	**Peak Area**			**% RSD**
	1	**2**	**3**	
1.97	2,012,329	1,502,758	1,934,591	15
3.94	9,437,088	8,665,399	9,935,793	7
24.6	90,926,720	81,302,960	87,712,119	6
49.3	170,877,681	189,410,278	181,726,138	5
73.9	265,131,856	243,721,136	267,737,025	5

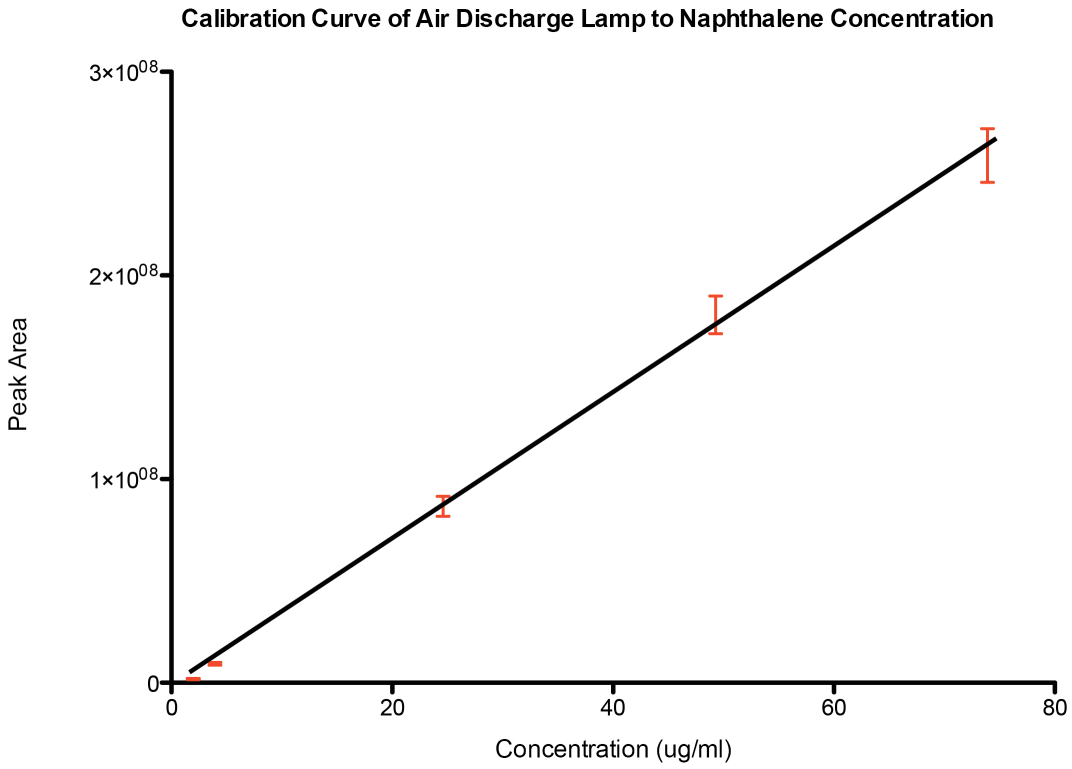

Figure 8: Analytical calibration curve of naphthalene to air discharge

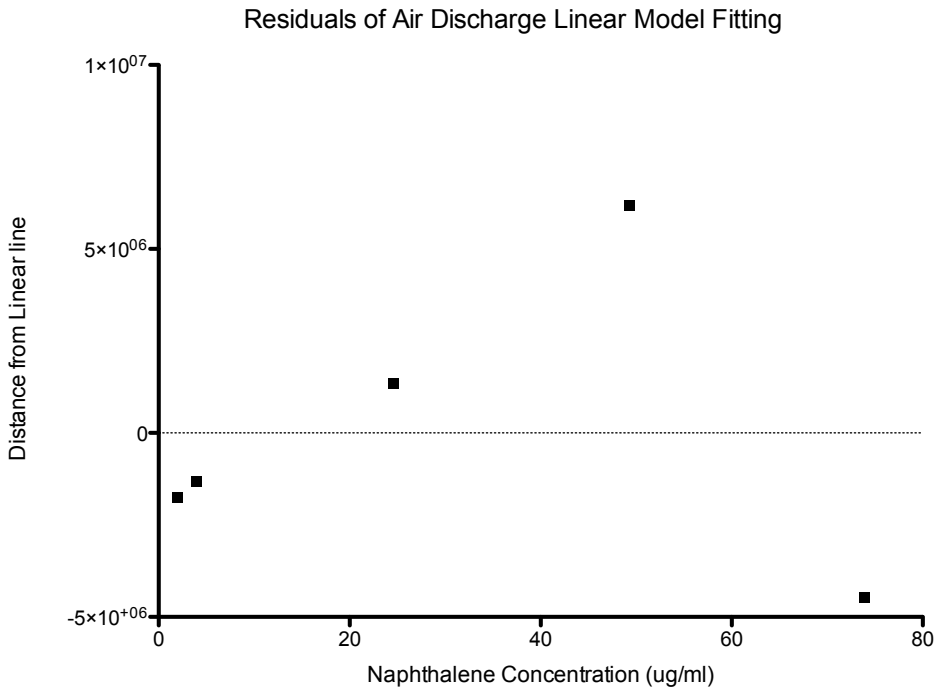

Figure 9: Residuals of naphthalene linear regression for air discharge

3.1.3.3 Helium discharge lamp

The results of the evaluation of the helium discharge lamp is given in Table 13. The helium discharge lamp had a limit of quantification less than 0.624 ug/ml. Peak area response was found to be linear from 0.624 ug/ml to 73.9 ug/ml with a correlation coefficient of 0.9936. The average percent relative standard deviation was 4% between the three replicate samples. The linear relation is defined by peak area = (4,110,000+/- 80,000) x [Naph Conc.] - (1,000,000 +/- 3,000,0000). An analytical calibration curve of peak area to concentration is given in Figure 10. The pattern of the residual analysis in Figure 11 indicates a non-linear relation between concentration and peak area for the helium LIS.

Table 13: Peak area as a function of naphthalene concentration

[Naphthalene] (ug/ml)	**Peak Area**			**% RSD**
	1	**2**	**3**	
0.624	773,995	743,697	800,806	4
0.984	1,046,226	1,028,982	1,042,337	0.9
1.97	4,417,981	4,620,392	4,726,839	3
3.94	10,351,792	9,079,291	9,627,322	7
24.6	100,527,144	108,993,472	111,952,704	6
49.3	209,137,312	218,302,480	223,180,860	3
73.9	297,153,856	283,781,848	291,109,332	2

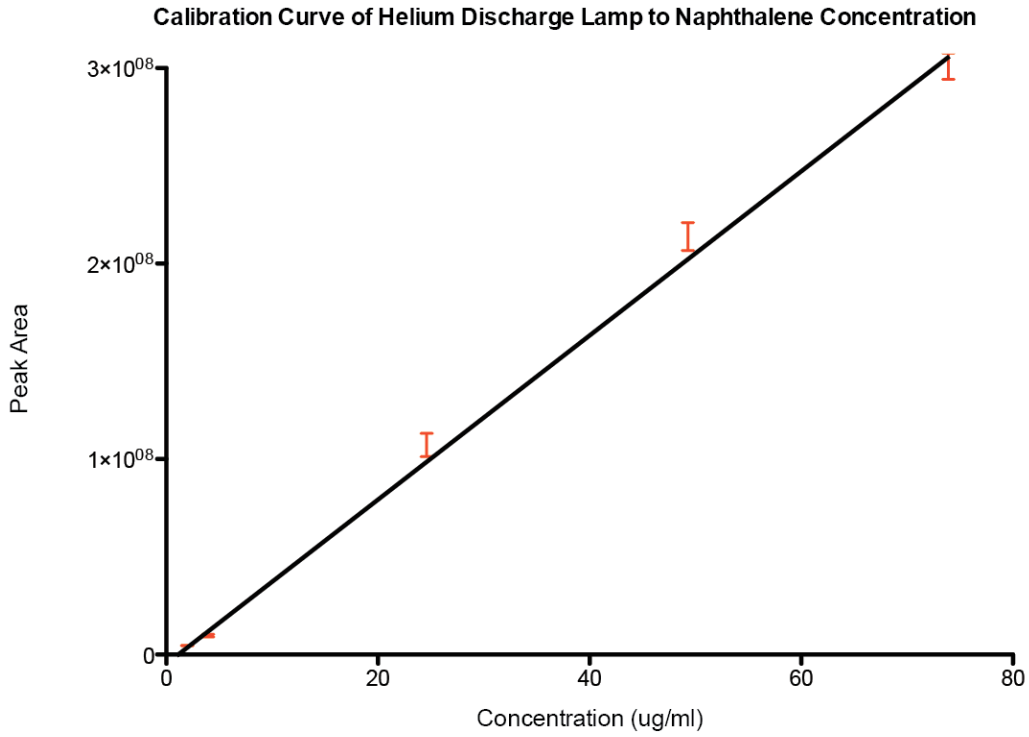

Figure 10: Analytical calibration curve of naphthalene to helium discharge

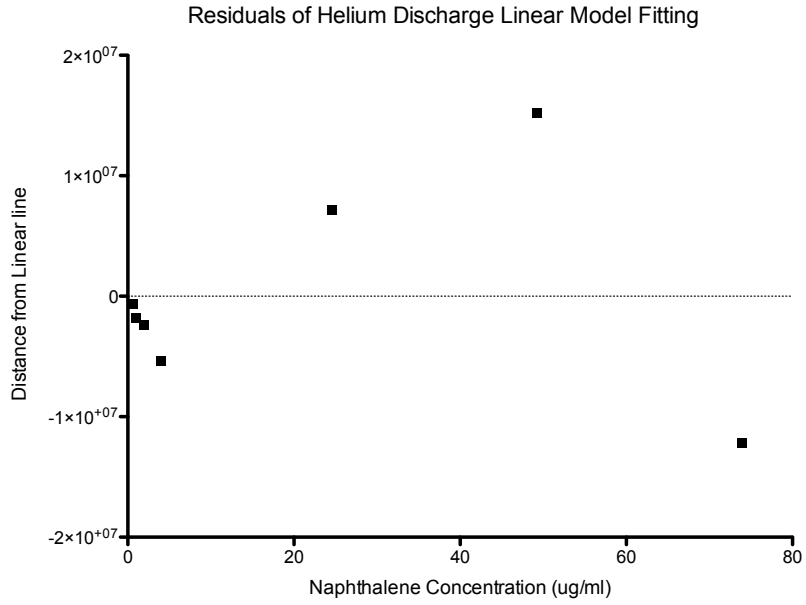

Figure 11: Residuals of naphthalene linear regression for helium discharge

3.1.3.4 Nitrogen discharge lamp

The results of the evaluation of the nitrogen discharge lamp is given in Table 14. The nitrogen discharge lamp had a limit of quantification less than 0.984 ug/ml. Peak area response was found to be linear from 0.984 ug/ml to 73.9 ug/ml with a correlation coefficient of 0.9968. The average percent relative standard deviation was 8% between the three replicate samples. The linear relation is defined by peak area = (4,270,000+/- 60,000) x [Naph Conc.] - (3,000,000 +/- 2,000,0000). An analytical calibration curve of peak area to concentration is given in Figure 12. The pattern of the residual analysis in Figure 13 indicates a linear relation between concentration and peak area for the nitrogen LIS.

Table 14: Peak area as a function of naphthalene concentration

[Naphthalene]	**Peak Area**			**% RSD**
(ug/ml)	**1**	**2**	**3**	
0.984	985,843	893,877	994,875	5
1.97	3,722,166	3,132,420	4,144,695	13
3.94	11,431,726	10,126,985	14,860,112	20
24.6	105,641,744	104,100,336	106,982,928	1
49.3	209,400,336	203,828,032	214,765,952	3
73.9	300,437,888	298,034,221	330,085,376	2

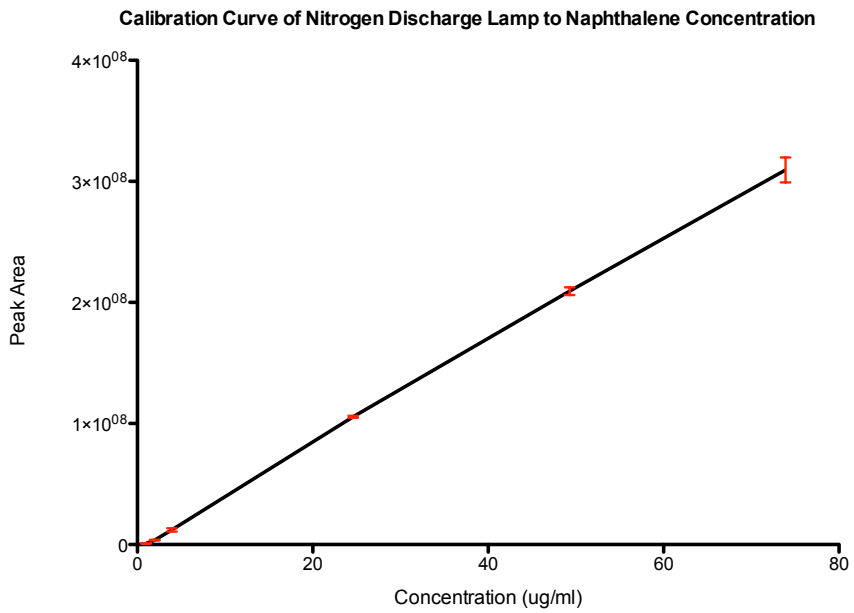

Figure 12: Analytical calibration curve of naphthalene to nitrogen discharge

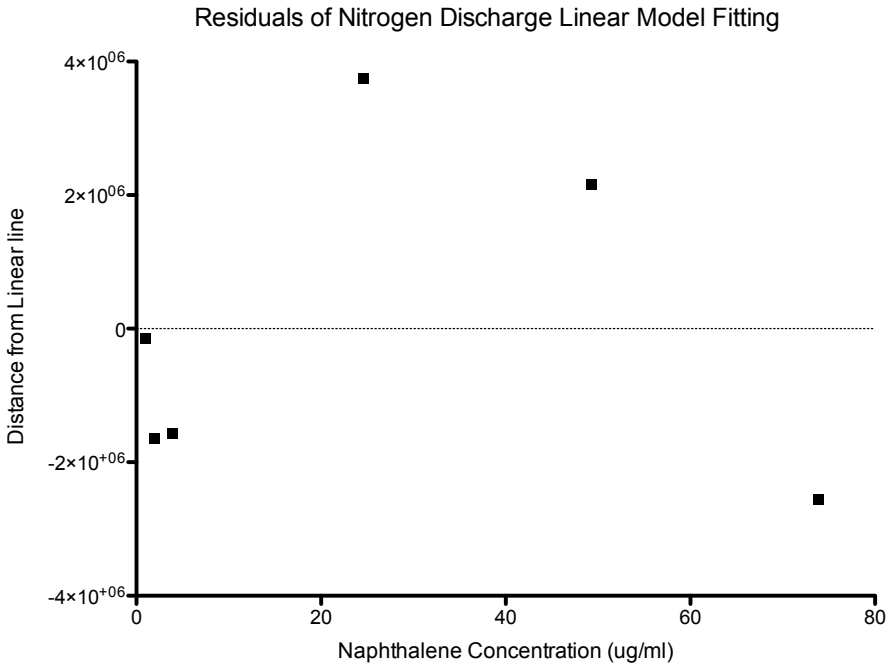

Figure 13: Residuals of naphthalene linear regression for nitrogen discharge

3.1.3.5 Argon discharge lamp

The results of the evaluation of the argon discharge lamp is given in Table 15. The argon discharge lamp had a limit of quantification less than 1.97 ug/ml. Peak area response was found to be linear from 1.97 ug/ml to 73.9 ug/ml with a correlation coefficient of 0.9943. The average percent relative standard deviation was 7% between the three replicate samples. The linear relation is defined by peak area = (4,270,000+/- 60,000) x [Naph Conc.] - (3,000,000 +/- 2,000,0000). An analytical calibration curve of peak area to concentration is given in Figure 14. The pattern of the residual analysis in Figure 15 indicates a linear relationship between concentration and peak area for the argon LIS.

Table 15: Peak area as a function of naphthalene concentration

[Naphthalene]	**Peak Area**			**% RSD**
(ug/ml)	**1**	**2**	**3**	
1.97	4,185,297	3,962,193	4,488,663	12
3.94	9,905,008	9,379,972	11,373,342	7
24.6	107,403,856	102,647,146	128,987,615	6
49.3	211,688,864	207,085,572	216,286,337	5
73.9	302,850,784	298,511,651	309,877,280	5

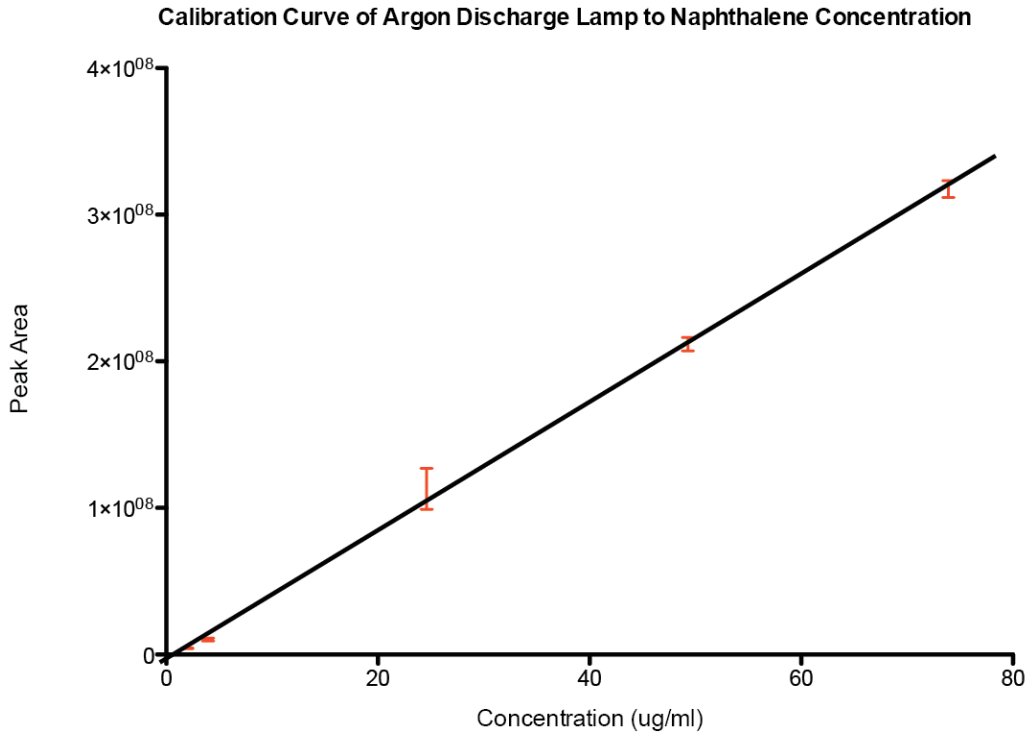

Figure 14: Analytical calibration curve of naphthalene to argon discharge

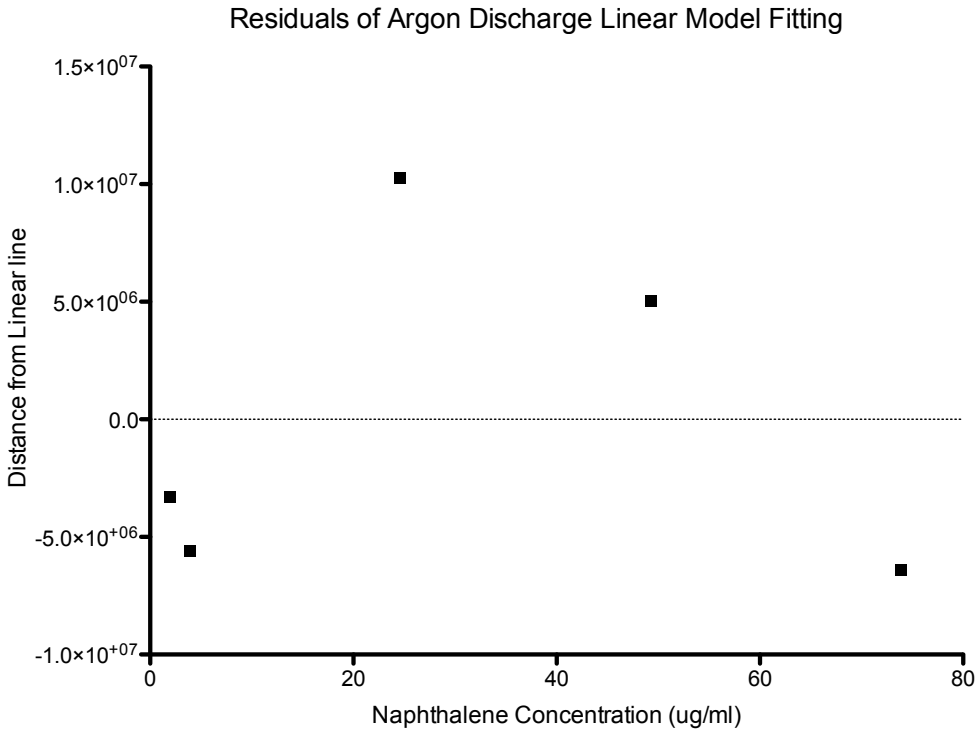

Figure 15: Residuals of naphthalene linear regression for argon discharge

3.1.3.6 Hydrogen discharge lamp

The results of the evaluation of the hydrogen discharge lamp is given in Table 16. The hydrogen discharge lamp had a limit of quantification less than 0.984 ug/ml. Peak area response was found to be linear from 0.984 ug/ml to 73.9 ug/ml with a correlation coefficient of 0.9760. The average percent relative standard deviation was 15% between the three replicate samples. The linear relation is defined by Peak Area = (4,600,000+/- 200,000) x [Naph Conc.] - (3,000,000 +/- 7,000,0000). An analytical calibration curve of peak area to concentration is given in Figure 16. The pattern of the residual analysis in Figure 17 indicates a non-linear relationship between concentration and peak area for the hydrogen LIS.

Table 16: Peak area as a function of naphthalene concentration

[Naphthalene] (ug/ml)	**Peak Area**			**% RSD**
	1	**2**	**3**	
0.984	1,294,011	1,588,879	1,077,721	20
1.97	4,190,329	4,898,725	3,917,152	12
3.94	10,651,292	8,044,139	12,998,573	23
24.6	111,462,552	115,996,350	96,599,609	9
49.3	211,413,136	248,299,176	260,890,731	11
73.9	321,106,176	369,864,798	279,838,803	14

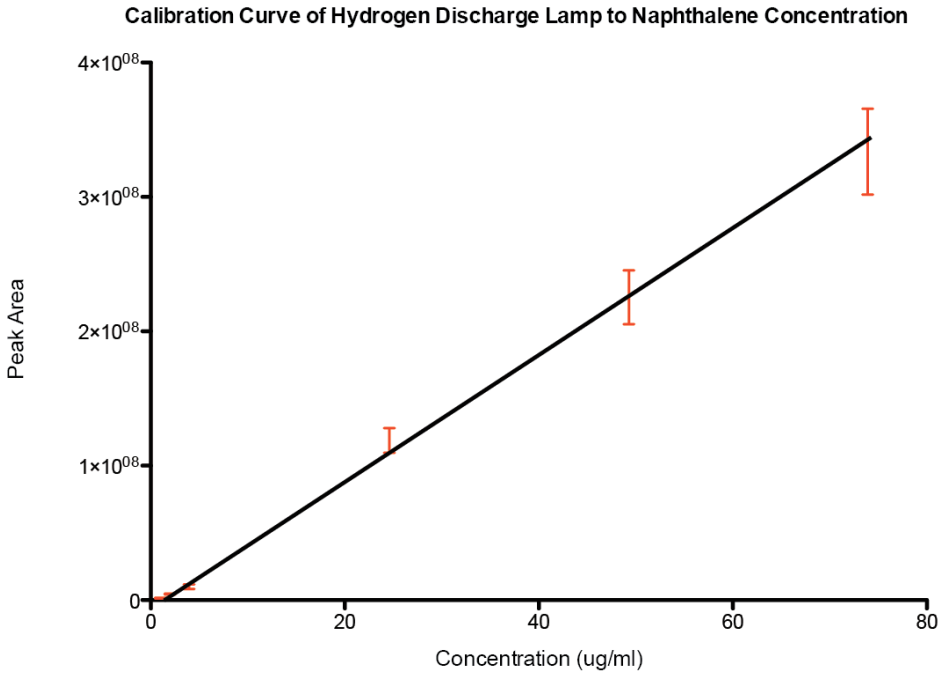

Figure 16: Analytical calibration curve of naphthalene to hydrogen discharge

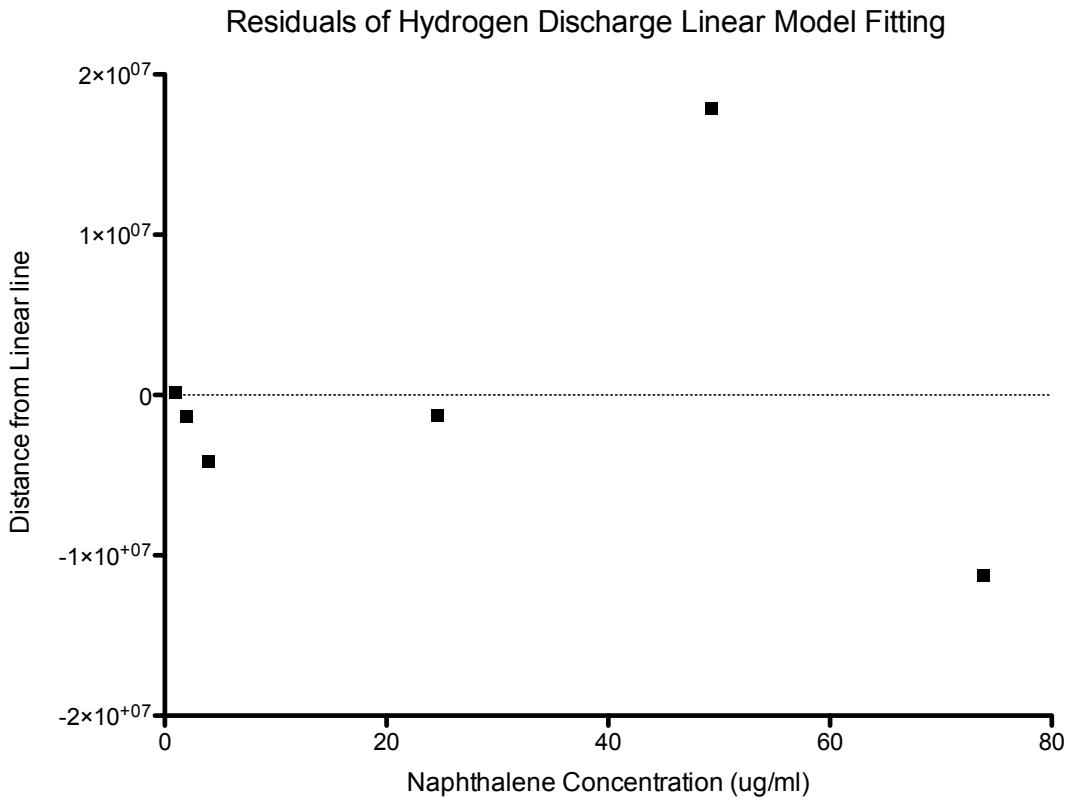

Figure 17: Residuals of naphthalene linear regression for hydrogen discharge

3.1.3.7 Oxygen discharge lamp

The results of the evaluation of the oxygen discharge lamp is given in Table 17. The oxygen discharge lamp had a limit of detection of than 0.078 ug/ml. Peak area response was found to be linear from 0.078 ug/ml to 73.9 ug/ml with a correlation coefficient of 0.9874. The average percent relative standard deviation was 16% between the three replicate samples. The linear relation is defined by Peak Area = (4,070,000+/- 90,000) x [Naph Conc.] - (3,000,000 +/- 4,000,0000). An analytical calibration curve of peak area to concentration is given in Figure 18. The pattern of the residual analysis in Figure 19 indicates a linear relation between concentration and peak area for the oxygen LIS.

Table 17: Peak area as a function of naphthalene concentration

[Naphthalene]	**Peak Area**			**% RSD**
(ug/ml)	**1**	**2**	**3**	
0.078	2,166,076	2,493,158	3,287,354	22
0.312	2,010,525	3,076,212	1,978,975	27
0.624	6,328,167	4,537,748	6,692,546	20
0.984	5,379,069	3,626,104	4,568,295	20
1.97	10,329,992	8,648,095	12,626,939	19
3.94	19,809,290	16,061,527	16,179,740	12
24.6	111,199,744	93,612,792	104,660,492	9
49.3	211,424,960	225,891,509	235,898,741	5
73.9	319,114,336	271,859,063	278,698,962	8

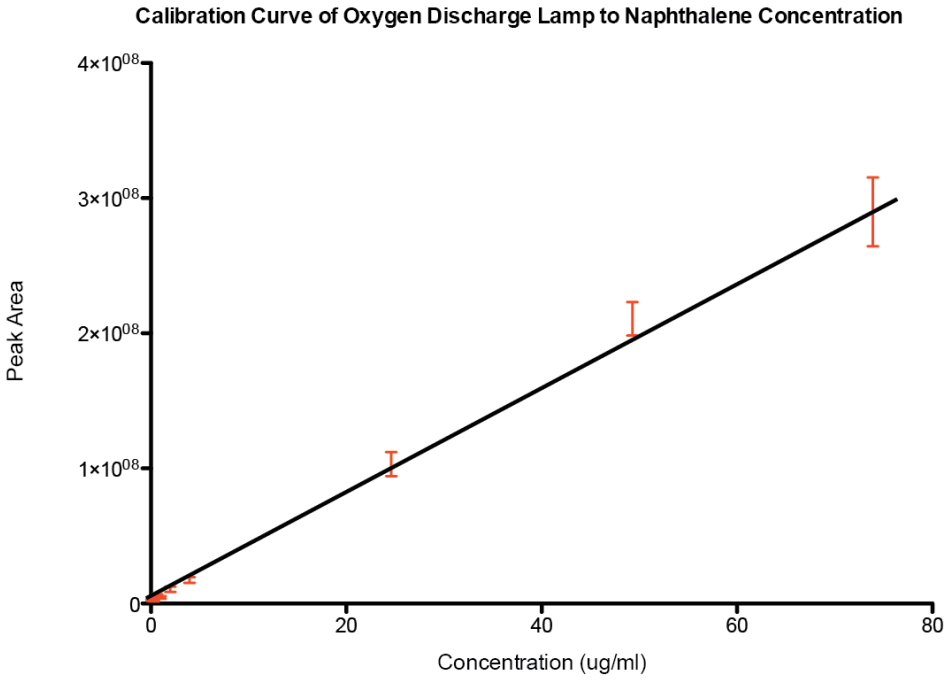

Figure 18: Analytical calibration curve of naphthalene to oxygen discharge

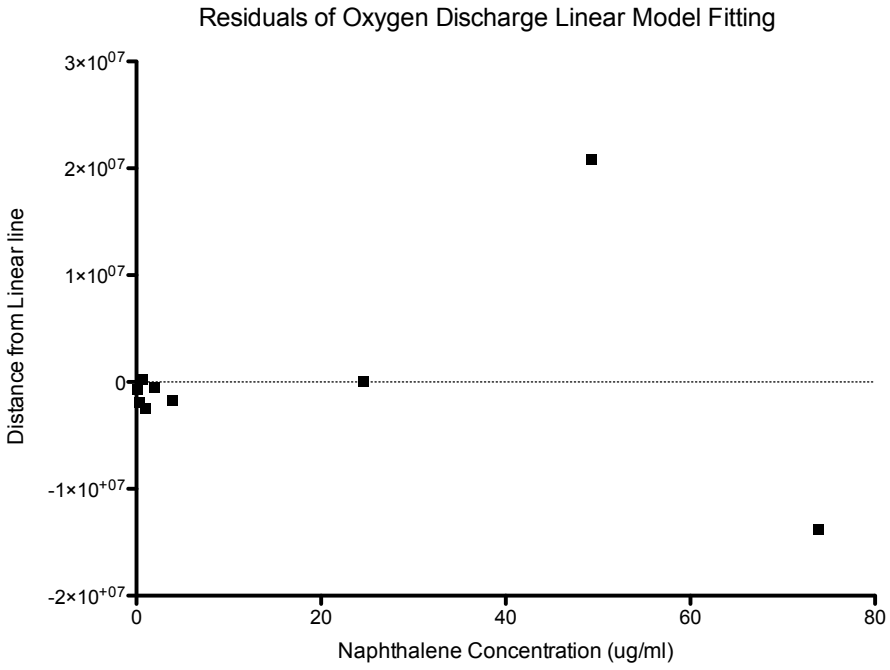

Figure 19: Residuals of naphthalene linear regression for oxygen discharge

3.1.3.8 Carbon dioxide discharge

The results of the evaluation of the carbon dioxide discharge lamp is given in Table 18. The carbon dioxide discharge lamp had a limit of detection of than 0.984 ug/ml. Peak area response was found to be linear from 0.984 ug/ml to 73.9 ug/ml with a correlation coefficient of 0.9945. The average percent relative standard deviation was 4.% between the three replicate samples. The linear relation is defined by peak area = (4,820,000+/- 90,000) x [Naph Conc.] - (7,000,000 +/- 4,000,0000). An analytical calibration curve of peak area to concentration is given in Figure 20. The pattern of the residual analysis in Figure 21 indicates a linear relationship between concentration and peak area for the carbon dioxide LIS.

Table 18: Peak area as a function of naphthalene concentration

[Naphthalene]	**Peak Area**			**% RSD**
(ug/ml)	**1**	**2**	**3**	
0.984	2,235,773	2,507,775	2,391,563	6
1.97	4,499,013	4,189,324	4,800,857	7
3.94	9,641,703	9,394,246	9,576,424	1
24.6	109,523,488	104,724,978	113,968,737	4
49.3	217,702,016	214,782,589	218,561,117	1
73.9	336,920,448	361,240,314	376,224,071	6

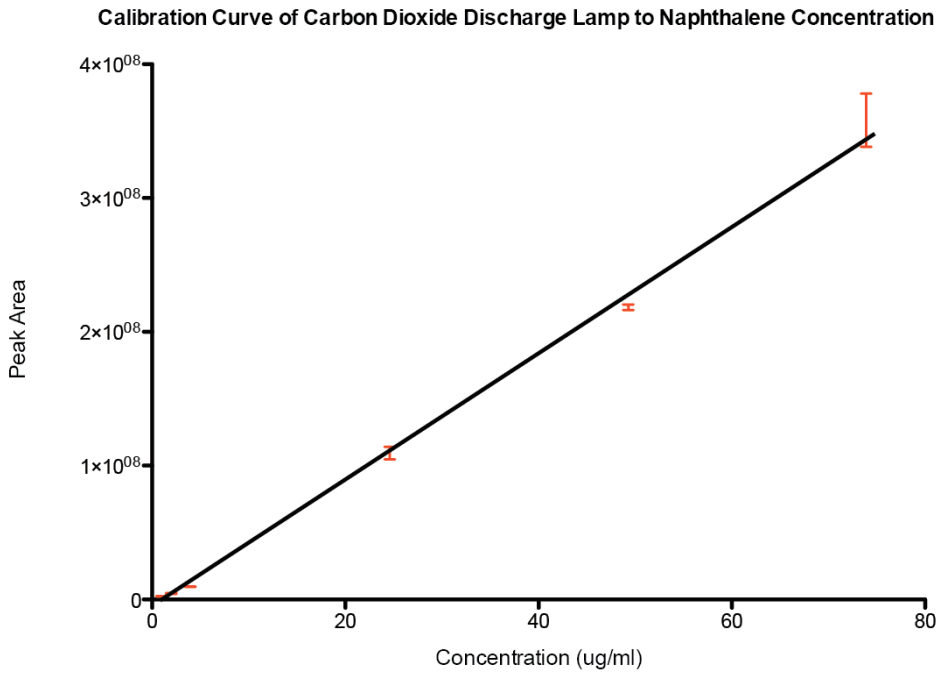

Figure 20: Analytical calibration curve of naphthalene to carbon dioxide discharge

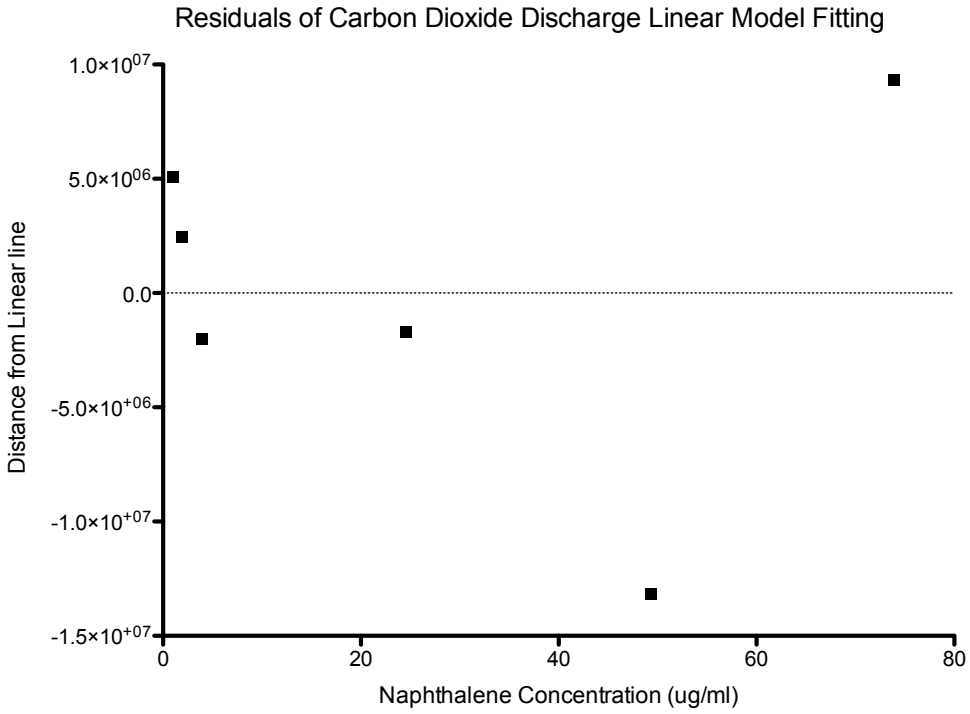

Figure 21: Residuals of naphthalene linear regression for carbon dioxide discharge

3.1.3.9 Analysis of variance

ANOVA was used to determine whether the naphthalene calibration curves from each of the gases were statistically different from one another. Generally, at lower concentrations the differing gases were non-discernable from one another. At higher concentrations of naphthalene differences were found to be significantly different between some gases. The commercial krypton lamp was found to be the most significantly different from the other LIS's. Generally, the commercial lamp had a lower limit of detection than the LIS sources, with the exception of oxygen. The correlation coefficient of the commercial lamp indicated a stronger linear relation between detector response and analyte concentration.

The response of an air discharge was significantly similar to nitrogen. This was expected as air contains a large majority of nitrogen and the emission spectra were similar. An unexpected result was seen comparing air and oxygen and air and helium. A significant difference in detector response was seen at 49.3 ug/ml but not at the concentrations above or below 49.3 ug/ml. This is a peculiar result that could be resolved with a larger number of replicates.

The lowest detected concentration was the same for both the air discharge and the nitrogen discharge. However, the sensitivity of the naphthalene to the air discharge was less than the nitrogen discharge. It is possible components, other than nitrogen, absorbed some of the photons leading to a less efficient ionization efficiency.

An analysis of variance of the peak area measurements was done at each concentration to determine whether the differences in measurements could be attributed to gas type or random variation. The results of the analysis is given in Table 19. Comparisons were made between peak areas for each gas at the eight concentration levels. In the case that no measurement was recorded a "-" signifies that no comparison was made. Gases that had no discernable ($p > 0.05$) differences are denoted "ns" and gases that had discernable differences are denoted "s".

Table 19: ANOVA of response to concentration

	Kr	**O_2**	**He**	**N_2**	**H_2**	**CO_2**	**Air**	**Ar**
Kr	-	ns, ns, ns, ns, ns, s, s, s	-, ns, ns, ns, ns, s, s	-, -, ns. ns, ns, s, s, s	-, -, ns, ns, ns, s, s, s	-, -, ns, ns, ns, s, s, s	-, -, -, ns, ns, s, s, s	-, -, -, ns, ns, s, s, s
O_2	-	-	-, ns, ns, ns, ns, ns, ns	-, ns, ns, ns, ns, ns, ns	-, -, ns, ns, ns, ns, ns, s	-, -, ns, ns, ns, ns, ns, s	-, -, -, ns, ns, ns, s, ns	-, -, -, ns, ns, ns, ns, ns
He	-	-	-	-, -, ns,	-, -, ns,	-, -, ns,	-, -, -,	-, -, -,

				ns, ns, ns, ns, ns	ns, ns, ns, ns, ns	ns, ns, ns, ns, s	ns, ns, ns, s, ns	ns, ns, ns, ns, ns
N_2	-	-	-	-	-, -, ns, ns, ns, ns, ns	-, -, ns, ns, ns, ns, s	-, -, -, ns, ns, ns, s	-, -, -, ns, ns, ns, ns
H_2	-	-	-	-	-	-, -, ns, ns, ns, ns, s	-, -, -, ns, ns, ns, s	-, -, -, ns, ns, ns, ns
CO_2	-	-	-	-	-	-	-, -, -, ns, ns, ns, s	-, -, -, ns, ns, ns, s
Air	-	-	-	-	-	-	-	-, -, -, ns, ns, ns, s

3.2 Thermally Assisted Vapour Introduction

3.2.1 TAVI mass spectra

In positive mode, the mass spectra of mode naphthalene, biphenyl, anthracene, phenanthrene, pyrene, fluoroanthrene, trans stilbene, rescorinol, salicylic acid, benzdiamine, ethyl-4-aminobenzoate all exhibited strong M^+ ion. Various novel organometallic compounds were found to be amenable with TAVI producing molecular ions. Figure 22 shows the mass spectrum of ferrocene. Ferrocene was found to have a high vapour pressure relative to the other compounds tested and only required temperatures of around 80°C before strong, dominant molecular peak was seen.

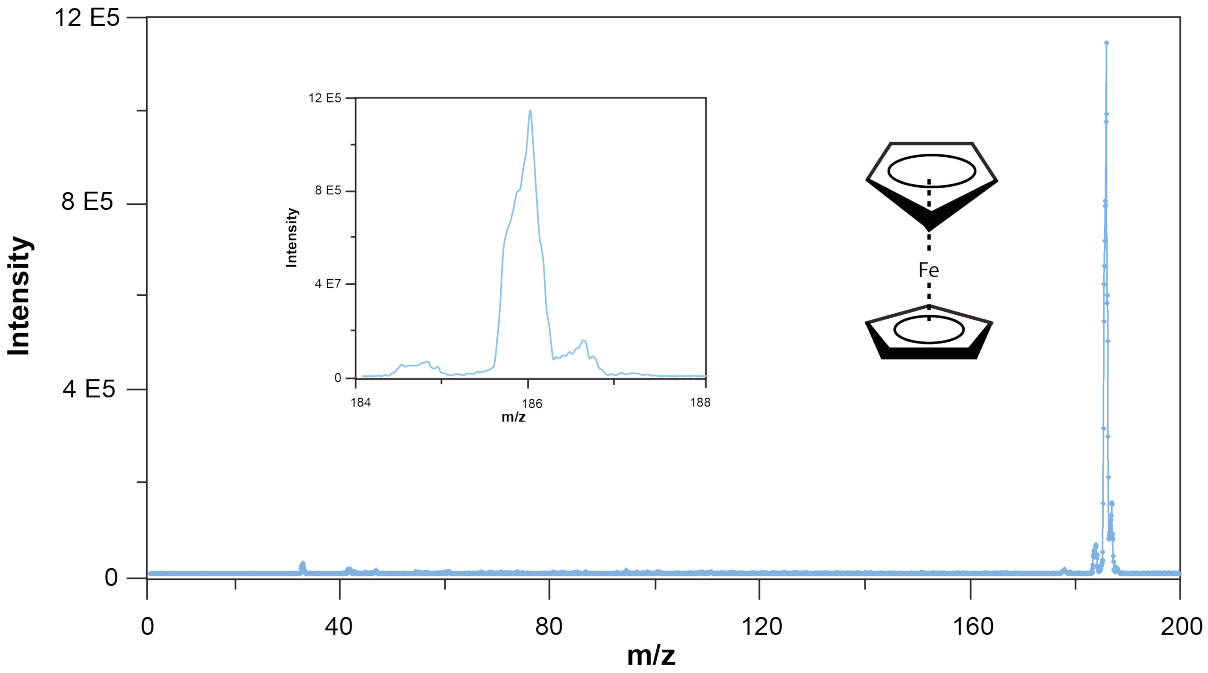

Figure 22: TAVI ms of Ferrocene

Structural information could be rationalized with TAVI APPI CID MS/MS. While high energy electron impact ionization is distinct from collision induced dissociation, fragmentation in both cases fragmentation is believed to be the result of internal energy distribution resulting in fragmentation. Comparisons between EI spectra and CID MS/MS showed general agreement to reference EI spectra. A compound with one of the strongest signals was ferrocene (molecular weight 186.04 amu) with an impressively strong molecular ion at m/z 186. CID on the molecular ion gave nearly identical mass spectra when compared to reference EI spectra. The parent ion could be fragmented to reveal loss of a ring group leaving and ion of m/z 121 easily identifiable as loss of a cyclopentadienyl ring seen in Figure 23.

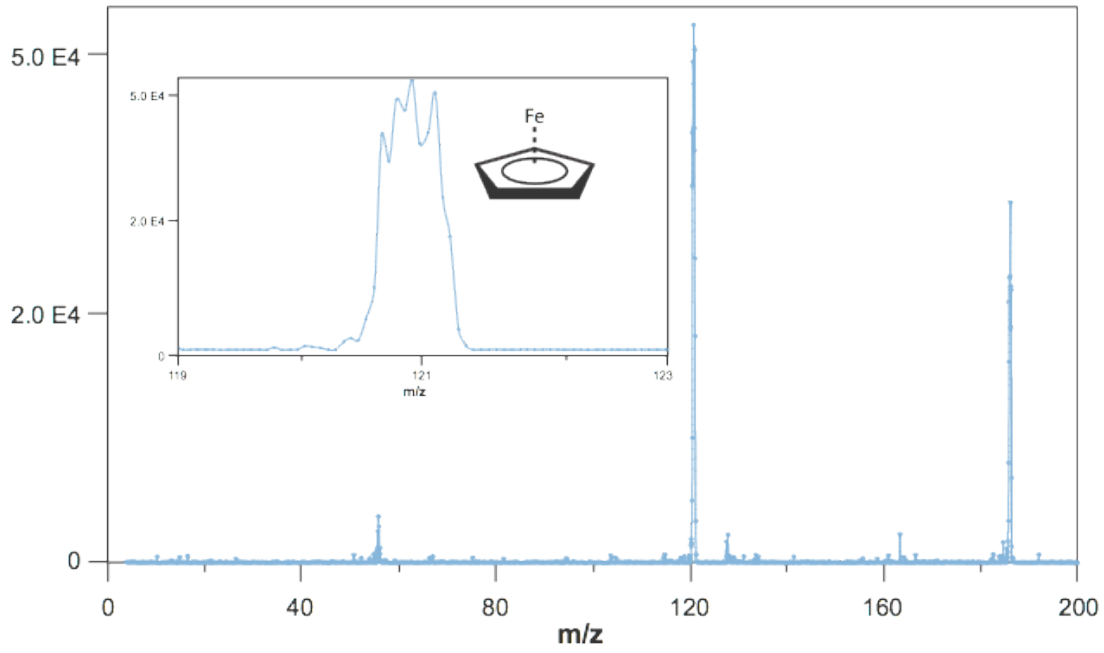

Figure 23: CID ms/ms Spectra of Ferrocene

The TAVI mass spectra of naphthalene is also dominated with molecular cation as shown in Figure 24.

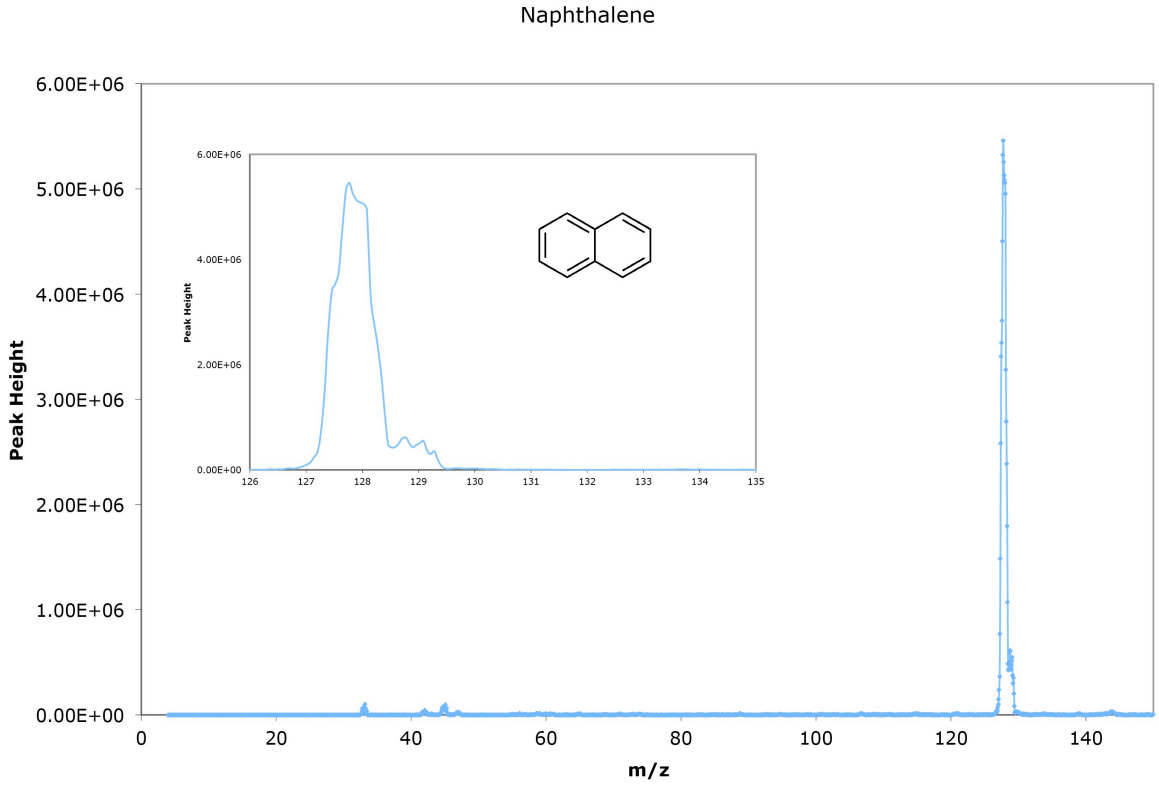

Figure 24: TAVI mass spectra of naphthalene

Figure 25 shows the TAVI mass spectra for biphenyl is dominated with the molecular ion.

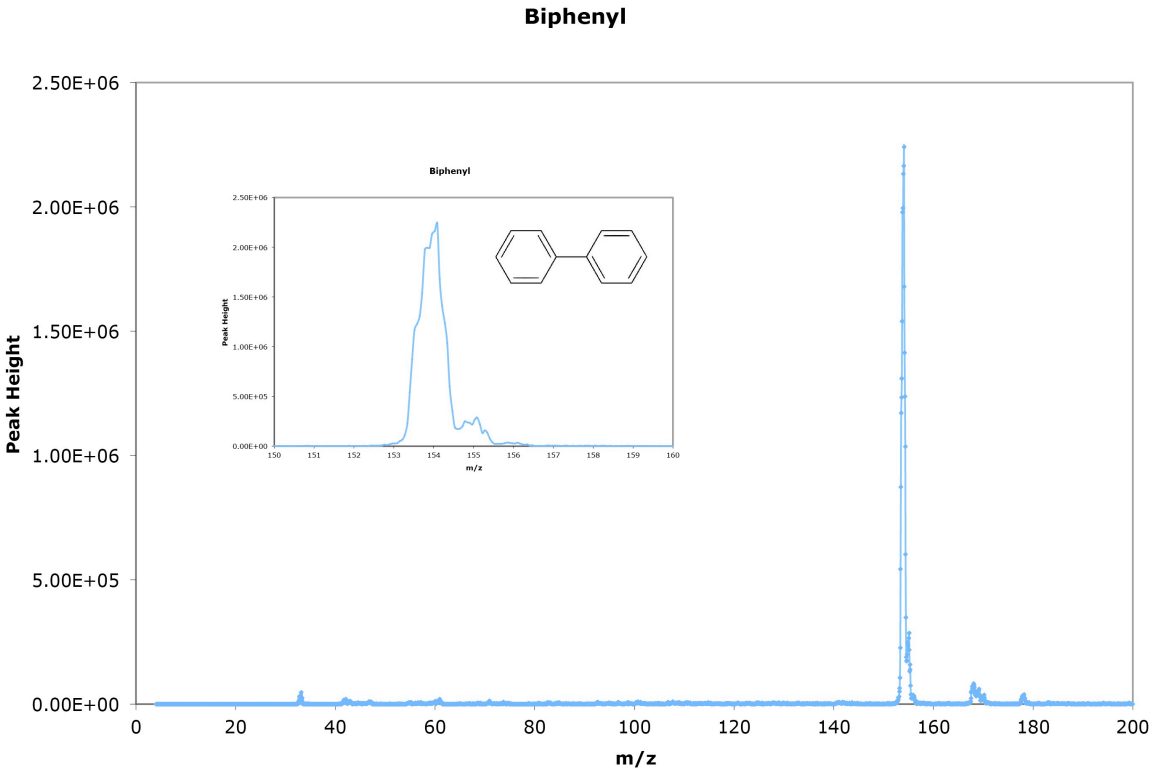

Figure 25: TAVI ms of biphenyl

$Cr(acac)_3$ had a strong molecular ion peak and when subjected to CID; readily produced expected daughter ions that corresponded to electron impact shown in Figure 27.

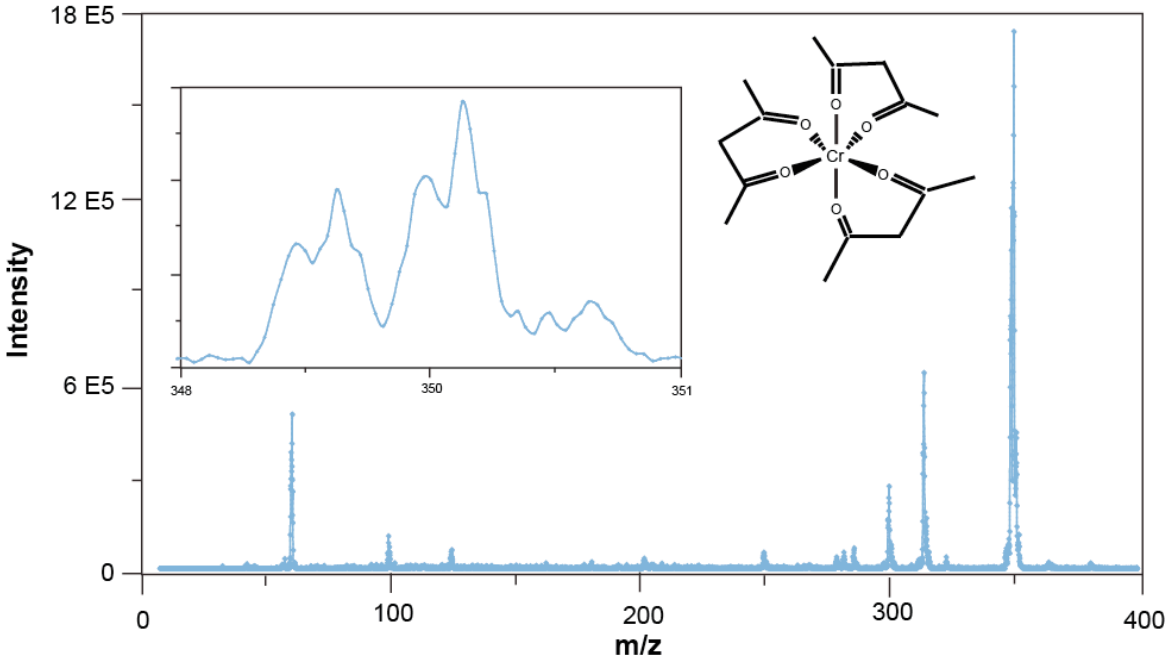

Figure 26: TAVI ms of $Cr(acac)_3$

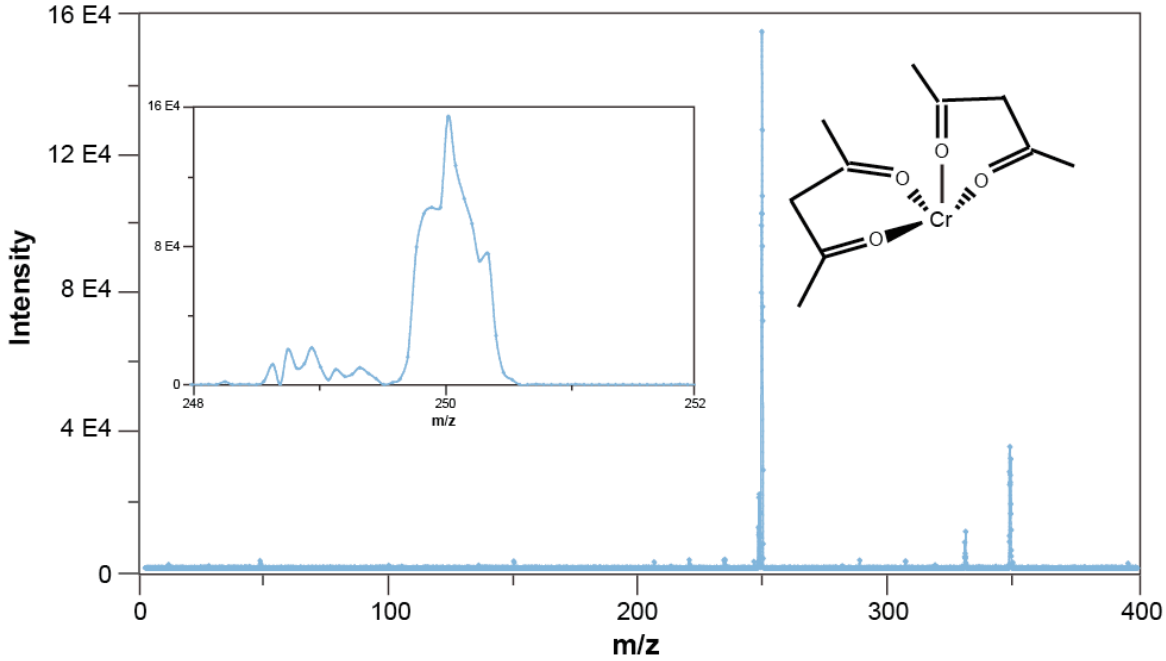

Figure 27: TAVI ms/ms of $Cr(acac)_3$

Not all compounds gave solely molecular ion peaks, $Fe(acac)_3$ for example had a very strong peak assigned as $[M+H\text{-}acac]^+$ ($[M - acac]^+$ peaks were seen by Hughes et al.) and also $Fe(acac)_3$ produced an ion assigned as $[2M\text{-}acac]^+$. A crude sample of $Cr(acac)_3$ exhibited mostly molecular peak as shown in Figure 26. With moderate collision energy one of the acac groups could be fragmented off leaving $[M\text{-}acac]^+$. Under more powerful CID conditions two acac groups could be removed. This selective fragmentation was useful in determining the identity of the components of the analyte.

To further validate the usefulness of the technique some novel synthetic compounds were tested. The crystal product of a synthesis, denoted as LG 113 (molecular weight 353.32 amu) ($C_{19}H_{13}F_2N_3O_2$) was found to have molecular cation of the desired product. Some of the other peaks revealed unused starting product and possible unwanted by products shown in figures 28 and 29. A reagent, fluorinated aniline, is easily seen in the TAVI mass spectrum at 111 amu in Figure 29.

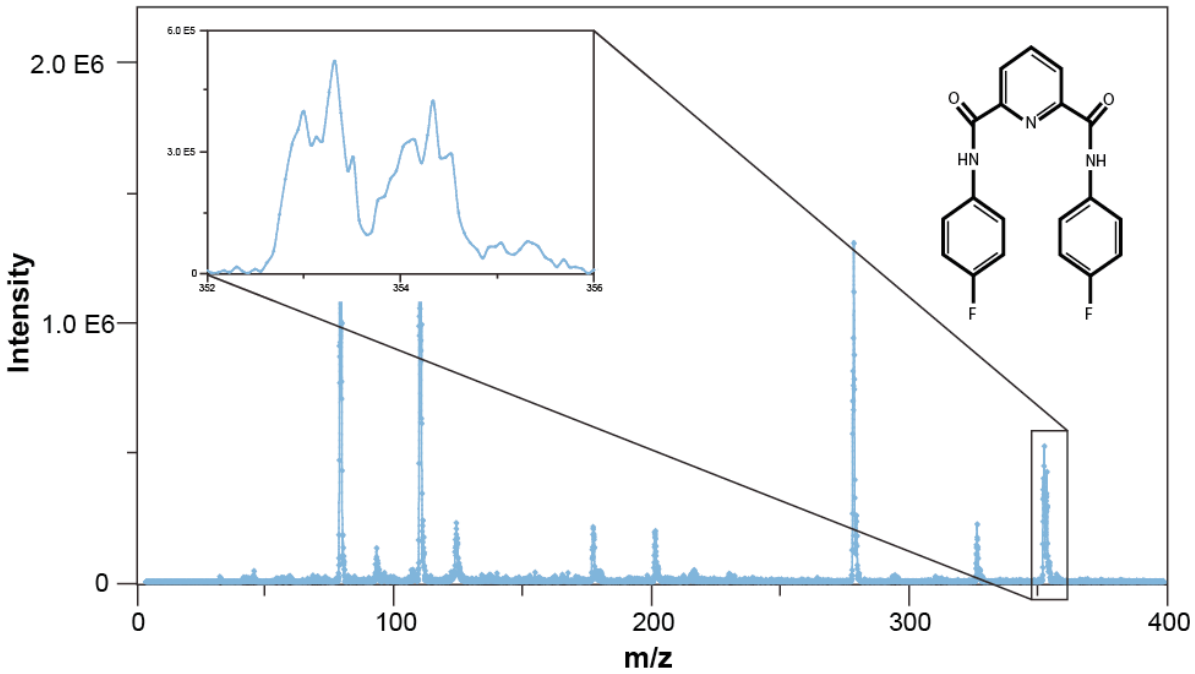

Figure 28: TAVI ms of LG113

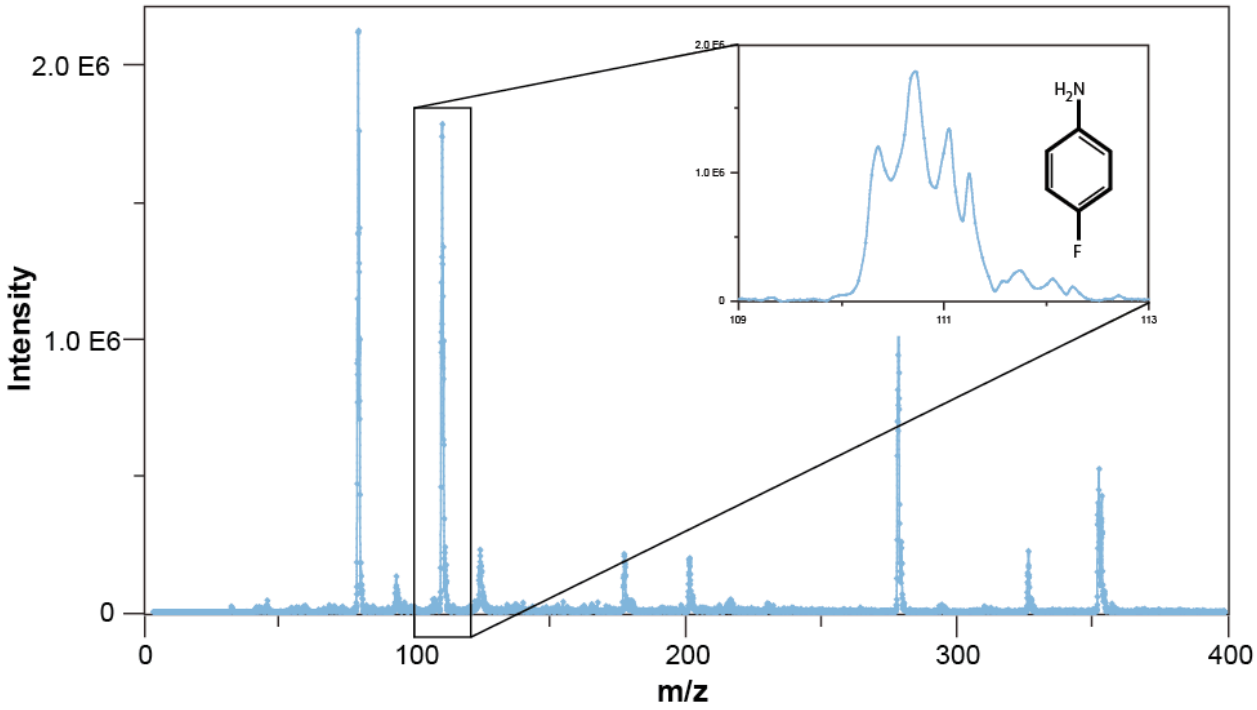

Figure 29: TAVI spectrum of LG113

In addition to identifying LG113, LG 159 with a molecular weight of 316.35 amu and a formula of $C_{20}H_{16}N_2O_2$ was ionized by TAVI as shown in Figure 30 with a $[M+H]^+$ peak.

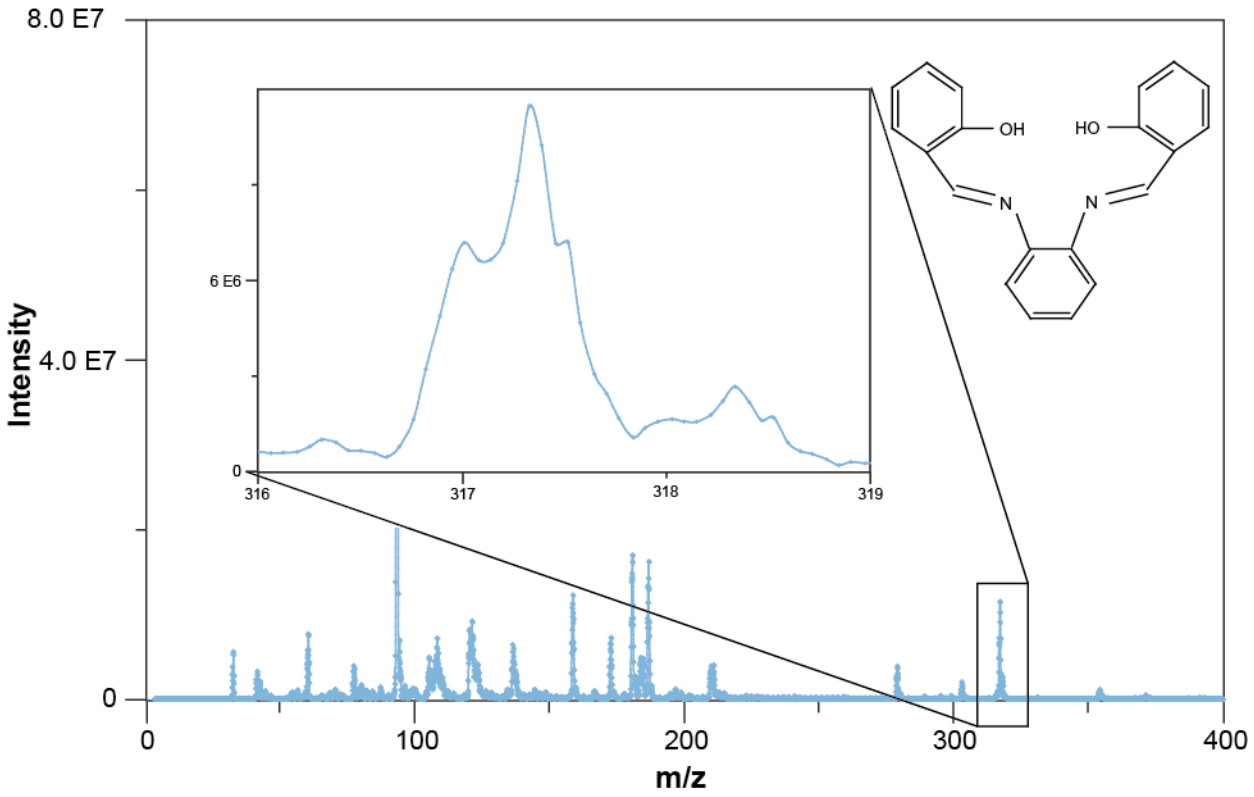

Figure 30: TAVI spectra of LG159

Chapter 4: Discussion

4.1 Lightning Ion Source

The LIS was constructed to be easily incorporated into the Waters Quattro Premier LC-MS/MS. The materials used were chosen to be as unreactive as possible to the high voltage and high temperature conditions. The tetrafluorinated ethylene discharge chamber was found to be largely resilient to the operating conditions but with prolonged use of sixty minutes or more the heat of the discharges turned the rigid material soft and pliable. Of the various electrode materials tested, the tungsten welding rods lasted the longest without any signs of disintegration. Electrodes made of copper wire of various diameters, stainless steel sewing needle, 2 mm plate steel were found to disintegrate showing signs of pitting within minutes. In contrast to other materials whose discharge was found to flicker, the discharge between two tungsten rods was found to be visually stable. The Emco DC/DC high voltage converter provided steady current levels for prolonged periods of time (0.30 +/- 0.01 amps). A range of other high voltage power supplies were tested but found to either short out or catch fire with less than 15 minutes of operation.

The use of several layers of polyolefin heat shrink tubing around the exposed electrodes outside of the discharge tube was essential in order to prevent arcing. It was found that the current could burn through three layers of tubing so five layers were used to insulate the welding rods.

4.1.1 Emission spectra

Many of the emission lines listed in the NIST reference spectra were found in the experimental results for each gas in the 200 to 960 nm range. A reference emission line was considered to have matched an experimental peak if the reference point fell within the range of a measured emission peak. Even though photons of wavelengths less than 200 nm could not be measured with the spectrometer it has previously been shown that high energy photons are produced from electrical discharges (Lyman, 1906; Hopfield, 1930; Tanaka et al., 1958) but given the optical properties of the lithium fluoride window it can be assumed that no photons with wavelength less than 105 nm made it out of the discharge chamber and be available for ionization. This does leave any photons of wavelength longer than 105 nm available for ionization.

Argon and nitrogen had the largest number of emission lines that matched as shown in figures 4 and 5. While the relative intensities of the measured lines did not match up to the reference spectra differences in discharge gas pressure and electrode distance have been found to produce different peak shapes and intensities (Lalos and Hammond, 1961; Abdel-Fattah, E., et al., 2011; Namba, S., et al., 2011). The LIS operates at approximately 1 atmosphere.

The emission profile of pure nitrogen discharge was found to have many shared emission peaks compared to the spectra of the air based discharge. Since the majority of air is nitrogen, this opens the possibility of using readily available air instead of nitrogen as a discharge gas.

4.1.2 Mass spectra

The LIS apparatus produced molecular ions. A representative polycyclic aromatic hydrocarbon, pyrene, produced primarily strong molecular ion or pseudo molecular ion ($[M+H]^+$) in both the lab and commercial source. The results of the LIS are in general agreement with other photon based ionization methods (Syage, J., 2004; Kersten, H., et al., 2009). Slight differences in the ratio of $M^+/[M+H]^+$ and $[M+2H]^+$ were found between the LIS and the commercial krypton lamp. While efforts were taken to match as many of the ion source parameters in an attempt to match the ion source energetics, perhaps the lack of a repeller plate on the LIS is responsible for the differences. It is noteworthy that the LIS produced a two-fold stronger response compared to the commercial APPI krypton discharge source. 17-α-hydroxyprogesterone produced similar $[M+H]^+$ spectra in the two techniques with the lab built source having a higher response factor. The increased signals from the lab built source may be due to a higher discharge current and possibly a more transparent lithium fluoride window (Gerasimova, N., 2006).

4.1.3 Calibration curve

In contrast to the recent atmospheric pressure photoionization literature (Robb et al., 2000), a variety of gases were able to ionize anaytes with similar analytical figures of merit as a krypton discharge lamp. A statistical analysis of the results found differences between the gases at higher concentrations but at lower concentrations no significant differences were found.

4.2 Demonstrating APPI for characterization of synthetic products

Using a Waters Quattro Premier LC MS/MS fitted with a Syagen PhotoMate™ photoionization lamp, samples of pure compounds and mixtures were heated using the TAVI device and the vapours released were monitored by APPI MS. This effectively generated molecular ions for the compounds tested. These spectra were easily generated within seconds. In addition to this, collision induced dissociation spectra were collected from some of these molecular ions. As it is demonstrated above, structural information and limited functional group analysis can be done using TAVI CID. Previously, vapours of pure aromatic compounds were photoionized in an effort to determine the mechanism of the formation of $[M+H]^+$ often seen in photoionization spectra (Syage, J., 2004) but this appears to be the first report of photoionizing vapours of organometallic compounds for structure determination. Similar techniques of ionizing analyte vapours have used other ionization methods like corona discharge in the case of Atmospheric Solids Analysis Probe (McEwen et al., 2009).

The impetus of this research grew from requests from a synthetic chemist who required confirmation of their synthetic reactions. Compound solubility and small sample size where two challenges presented. TAVI does not require a liquid sample solution and could easily determine the molecular weights of insoluble organometallic crystals with minimal sample preparation. Solid samples were tapped into a glass melting point capillary tube which was resistively heated directly below the photoionization lamp. Liquid samples could be either injected in a heated glass capillary tube or spotted onto a lithium fluoride plate that was held directly in front of the photoionization lamp. TAVI APPI MS/MS offers simple mass spectra dominated by molecular ion, M^+, signals compared to solvent based APPI which generally leads to $[M+H]^+$. To demonstrate the

effectiveness of TAVI APPI MS/MS, a range of PAH and organometallic compounds were examined. For the majority of compounds molecular ions were observed as demonstrated by spectra of naphthalene, pyrene and ferrocene.

In addition to molecular weight information, collision induced dissociation offered information about the structure on the compounds. For example, ferrocene could be fragmented to lose one of the five membered rings. $Cr(acac)_3$ could be selectively fragmented to lose one or two of the acac groups yielding structural information.

There have been various recent attempts to find an appropriate mass spectrometric techniques to analyze organometallic and coordination compounds. Previous work by Dorcier et al. using photoionization on organometallic compounds dissolved in solvents produced mixed results; molecular ions were observed but significant toluene substitution, analyte methylation and various unidentified peaks were also observed (Dorcier et al., 2006). A "solvent-free" technique is desirable for insoluble compounds or compounds that may dissociate in solution. The technique described here meets that objective. A recent paper by Hughes et al. reported success with the use of MALDI-TOFMS on organometallic and coordination compounds (Hughes et al., 2009). For most of the compounds evaluated, strong molecular ions were observed, but sodium and potassium adducts were also observed. As demonstrated by Syage, 2004, vapours examined by APPI generate molecular ions (M^+)

Carrying on from this preliminary work, several aspects of the thermally assisted vapour introduction technique could be refined to allow for analysis of air sensitive compounds and

quantitative measurements. The suitability of sequential thermal desorption could be investigated for multicomponent samples.

Chapter 5: Conclusions

5.1 Summary

The overall goal of this thesis was to examine the validity of two separate hypothesis both dealing with atmospheric pressure photoionization: To determine whether a variety of common gases could be used as discharge gases for ionization; and whether photoionization of vapours generated from solid samples could allow molecular weight determination and some structural information.

5.2 Lightning Ion Source

The inexpensive Lightning Ion Source has shown that it can be used to identify molecular masses and determine some functional groups in test compounds. The results of the three sets of analysis; photon emission profile, mass spectra with M^+ and $[M+H]^+$ and comparable analytical response to the commercial lamp, demonstrate its usefulness.

Using the custom fabricated LIS it was found that photons produced from an electrical discharge in all of the gases tested could photoionize a variety of test compounds. The LIS was different from commercial photoionization sources in two important ways. The LIS had a discharge at atmospheric pressure whereas the two commercial sources are both contain low pressure discharge chambers. Additionally, the LIS was found to be effective with a variety of discharge gases whereas the commercial sources specifically use krypton as the discharge gas. Significant differences were found between the response to the analytes depending on the discharge gas used. The majority of the discharge gases used in the LIS had greater sensitivity but lower limit of

detection when compared to the krypton lamp. Additionally, the mass spectra generated by the LIS did exhibit difference ratios of $M^+/[M^+H]^+/[M+2\ amu]^+$ but in many ways the inexpensive LIS was found to be a powerful tool comparable to the commercial source.

Carrying on from this preliminary work, several aspects of the LIS could be refined. For instance, the effect on electrode distance and position has on photon flux and subsequent ionization could be examined to maximize ionization. Related to electrode orientation, discharge current could be examined to identify an optimum current for maximum ionization. Further testing to evaluate the applicability of the source may be useful to produce an inexpensive ion source for use on any atmospheric pressure ionization mass spectrometer.

Applications such as petrochemical analysis or screening for explosives in security applications maybe useful, especially with the finding that common air can be used as a discharge gas giving similar analytical results to commercial photoionization techniques. The US Transportation Safety Administration is responsible for screening over 700 million passengers and support staff annually at a cost of over one billion dollars (Elias, B., 2009). A key requirement is the screening of explosives and drugs of abuse, two applications well suited to photoionization (Syage, J., 2006). Most interesting, is the use of the LIS for remote or field analysis. With air being an effective discharge gas, LIS may be useful in field analysis where operating supplies are hard to obtain.

5.3 Thermally Assisted Vapour Introduction

Using a custom configured heating apparatus to produce vapours of a range of test compounds thermally assisted vapour introduction was found to offer rapid characterization without solvents. In instances where samples are not soluble in common solvents or when limited sample size is an issue TAVI may be an effective method to determine molecular weight and even determine some functional group information quickly.

Carrying on from this preliminary work, several aspects of the thermally assisted vapour introduction technique could be refined to allow for analysis of air sensitive compounds and quantitative measurements. For air sensitive compounds analytes can be sealed within a melting point tube and inserted into the TAVI apparatus. It is likely that the source block could be flooded with an inert gas displacing the offending oxygen. The melting point tube could be heated and broken to release the vapours into the inert environment of the source block where they could be ionized by photons. Another avenue of future development could be to determine the suitability of sequential thermal desorption that could be used for multicomponent samples.

References

Abdel-Fattah, E., Bazavan, M., Sugai, H., Langmuir probe diagnostics of electron energy distributions with optical emission spectroscopy in capacitively coupled rf discharge in nitrogen, J. Appl. Phys., 113303-8, 2011.

Al- Joboury, Turner, D., Molecular Photoelectron Spectroscopy. Part I The Hydrogen and Nitrogen Molecules, 5141- 5147, 1963.

Andrade, F., Wetzel, W., Chan, G., Webb, M., Gamez, G., Ray, S., Hieftje, G., A New, Versatile, Direct- Current Helium Atmospheric- Pressure Glow Discharge, J. Am. At. Spectrom., 21, 1175-1184, 2006.

Antonov, V., Letokhov, V., Shibanov, A., Formation of Molecular Ions as a Result of Irradiation of the Surface of Molecular Crystals by UV laser Radiation, 441-444, 1980.

Banning, M., The Far Ultraviolet Refectivities of Metallic Films, J. O. S. A., 32, 98-102, 1942.

Borsdorf, H., Nazarov, E., Miller, R., Time-of-Flight Ion Mobility Spectrometry and Differential Mobility Spectrometry; A Comparative study of their efficiency in the analysis of halogenated compounds, Talanta, 71, 1804-1812, 2007.

Bos, B., van Leeuwan, S., Karst, U., From Fundamentals to Applications: Recent Developments in Atmospheric Pressure Photoionization Mass Spectrometry, Anal. Bioanal. Chem., 384, 85-99, 2006.

Brion, C., An Improved Mass Spectrometer Photoionization Source, Analytical Chemistry, 38, 1941-1942, 1966.

Clark, I., Frost, D., A Study of the Energy Levels in Benzene and some Fluorobenzenes by Photoelectron Spectroscopy, J. Am. Chem. Soc, 89, 244-247, 1966.

Cody, R., Laramée, J., Durst, H., Versatile New Ion Source for the Analysis of Materials in Open

Air Under Ambient Conditions, Anal. Chem, 77, 2297-2302, 2005.

Ditchburn, R., Arnot, F., The Ionisation of Potassium Vapour, Proc Royal Soc, 516- 536, 1929.

Dorcier, A., Dyson, P., McIndoe, J., Analysis of Coordination and Organometallic Compounds using Photoionization Mass Spectrometric Techniques, Eur. J. Inorg. Chem, 4294-4297, 2003.

Driscoll, J., Photoionization Monitor for Oxides of Nitrogen, US Patent 40,359/72, 1972.

Driscoll, J., Warneck, P. , The Analysis of PPM Levels of Gases in Air by Photoionization Mass Spectrometry, Journal of the Air Pollution Control Association, 23, 858- 863, 1973.

Druyvesteyn, M., Penning, F., The Mechanism of Electrical Discharges in Gases of Low Pressure, Reviews of Modern Physics, 12, 87- 175, 1940.

Duncanson, A., Stevenson, W., Some Properties of Magnesium Fluoride Crystallized from the Melt, 1001-1006, 1958.

Eelman, M., Blacquiere, J., Moriarty, M., Fogg, D., et al., Shining New Light on an Old Problem: Retooling MALDI Mass Spectrometry for Organotransition-Metal Catalysis, Chem. Int. Ed., 303-306, 2008.

Einstein, A., On a Heuristic Point of View about the Creation and Conversion of Light. Translated by Haar, D.

Elias, B., Airport Passenger Screening: Background and Issues for Congress, Congressional Research Service, 2009.

Frost, D., McDowell, C., Vroom, D., Photoelectron Kinetic energy Analysis in Gases by means of Spherical Analyser, Proceedings of the Royal Society of London. Series A, Mathematical and Physical Sciences, 296, 566-579 , 1967.

Gerasimova, N., CaF2, MgF2, SiO2, Al2O3, SiC, LiF, BaF2, and ZrO2 Optical Single Crystals

used in Studies in the VUV Spectral Region, Instruments and Experimental Techniques, 49, 408-412, 2006.

Gurley, N. Beloukhina, K. Boudreau, A. Klegeris, W. S. McNeil, The Synthesis and Characterization of a Series of Cobalt(II) β-Ketoaminato Complexes and Their Cytotoxic Activity Towards Human Tumor Cell Lines, J. Inorg. Biochem., 105, 858-866, 2011.

Gross, M., Caprioli, R., The Encyclopedia of Mass Spectrometry, Elsevier, Vol 6, 2007.

Gyulai, Z., Die Dispersion Einiger Alkalihalogenide im Ultravioletten, 80-87, 1927.

Haapala, M., Pól, J., Saarela, V., Kotiaho, T., Ketola, R., Franssila, S., Kauppila, T., Kostainen, R., Desorption Atmospheric Pressure Photoionization, Anal. Chem, 79, 7867- 7872, 2007.

Harper, J., Charipar, N., Mulligan, C., Zhang., X., Cooks, G., Ouyang., Low-Temperature Plasma Probe for Ambient Desorption Ionization, Anal. Chem., 9097-9104, 2008.

Hass, G., Tousey, R., Reflective Coatings for the Extreme Ultraviolet, J. Opt. Soc Am., 49, 593-602, 1959.

Herzog, R., Marmo, F., Mass Spectroscopic Determination of Photoionization Products, The Journal of Chemical Physics, 27, 1202-1205, 1957.

Hopfield, J., Absorption and Emission Spectra in the Region l600-1100, Phys. Rev, 1133-1134, 1930.

Hopfield, J., New Ultra-violet Spectrum of Helium, The Astrophysical Journal, 72, 133-150, 1930.

Huffman, R., Larrabee, J., Tanaka, Y., Rare Gas Continuum Light Sources for Photoelectric Scanning in the Vacuum Ultraviolet, Applied Optics, 4, 1581-1588, 1965.

Hughes, L., Wyatt, M., Stein, B., Brenton, A., Investigation of Solvent-Free MALDI-TOFMS Sample Preparation Methods for the Analysis of Organometallic and coordination Compounds, Anal. Chem., 81, 543-550, 2009.

Jensen, C., Libby, W., Intense 584-Å, Light from a Simple Continuous Helium Plasma, 135, 1247-1252, 1964.

Jones, E., Harrison, A., Asymmetric Charge Transfer Reactions of Rare Gas Ions at Low Ion Energies, Int. J. Mass Spectrom. Ion Phys., 6, 77-88, 1971.

Kato, R., Optical Properties of LiF in the Extreme Ultraviolet, 2525-2533, 1961.

Kato, R., Nakashima, S., Optical Properties of Irradiated LiF Crystals in the Extreme Ultraviolet Region, J. Phys. Soc. Japan, 15, 2111-2112, 1960.

Kauppila, T., Kuuranne, T., Meurer, E., Eberlin, M., Kotiaho, T., Kostiainen, R., Atmospheric Pressure Photoionization Mass Spectrometry. Ionization Mechanisms and the Effect of Solvent on the Ionization of Naphthalenes, Anal. Chem, 74, 5470-5479, 2002.

Kersten, H., Funcke, V., Lorenz, M., Brockmann, K., Benter, T., O'Brien, R., Evidence of Neutral Radical Induced Analyte Ion Transformation in APPI, and Near-VUV APLI, J. Am. Chem. Soc, 2009, 1868-1880, 2009.

Kinsinger, J., Stebbings, W., Valenzi, R., Taylor, J., Spectral Evaluation of a Sealed Helium Discharge Lamp for Studies in Photoelectron Spectroscopy, Anal. Chem, 44, 773-777, 1972.

Kiser, R., Introduction to Mass Spectrometry and its Applications, Prentice-Hall Inc, 1965.

Lalos, G., Hammond, G., Emission Spectra of Hot Dense Gases, 616-627, 1961.

Lorenz, M., Schiewek, R., Brockman, K., Schmitz, O., Gäb, S., Benter, T., The Distribution of Ion Acceptance in Atmospheric Pressure Ion Sources: Spatially Resolved APLI Measurements, J. Am Soc Mass Spectrom, 19, 400-410, 2008.

Lossing, F., Tanaka, I., Photoionization as a Source of Ions for Mass Spectrometry, J. Chem. Phys., 25, 1031-1034, 1956.

Lubben, A., McIndoe, J., Weller, A., Coupling an Electrospray Ionization Mass Spectrometer with

a Glovebox: A Straightforward, Powerful, and Convenient Combination for Analysis of Air-Sensitive Organometallics, Organometallics, 3303-3306, 2008.

Lyman, T., The Spectrum of Hydrogen in the Region of Extremely Short Wave-length, The Astrophysical Journal, 23, 181- 214, 1906.

Lyman, T., The Spectrum of Helium in the Extreme Ultra-violet, Science, 59, 422, 1924.

Lyman, T., The Spectrum of Helium in the Extreme Ultra-violet, Nature, 113, 785, 1924.

Lyman, T., The Spectrum of Helium in the Extreme Ultra-violet, The Astrophysical Journal, 60, 1-15, 1924.

Lyman, T., On the Spectra of Neon and Argon in the Extreme Ultra-violet, Nature, 116, 358, 1925.

Lyman, T., Saunders, F., The Spectrum of Neon in the Extreme Ultra-violet. Proc. N. A. S., 12, 92-96, 1926.

Madden, R., Canfield, L., Apparatus for the Measurement of Vacuum Ultraviolet Optical Properties of Freshly Evaporated Films, Journal of the Optical Society of America, 51, 838-845, 1961.

McEwen, C., McKay, R., Larsen, B., Analysis of Solids, Liquids, and Biological Tissues Using Solids Probe Introduction at Atmospheric Pressure on Commercial LC/MS Instruments, 2005, 7826-7831, 2005.

McEwen, C. and Larsen, B., Ionization Mechanisms Related to Negative Ion APPI, APCI, and DART, J am Soc Mass Spectrom, 1518-1521, 2009.

Milgram, A., Givens, M., Extreme Ultraviolet Absorption by Lithium Fluoride, Phys. Rev, 125, 1506-1509, 1962.

Millikan, R., Bowen, I., Extreme Ultra-violet Spectra, The Physical Review, 23, 1-38, 1924.

Namba, S., Yamasaki, T., Hane, Y., Fukuhara, D., Kozue, K., Takiyama. K., Emission

spectroscopy of a microhollow cathode discharge plasma in helium-water gas mixtures, J. Appl. Phys., 073307-5, 2011.

NIST Webbook (2009). Atomic Spectra Database. Retrieved from http://www.nist.gov/pml/data/asd.cfm.

Nordling, C., Sokolowski, E., Siegbahn, K., Precision Method for Obtaining Absolute Values of Atomic Binding Energies, Phys. Rev, 105, 1676-1677, 1957.

Patterson, D., Vaughan, W., Influence of Crystal Surface on the Optical Transmission of Lithium Fluoride in the Vacuum- Ultraviolet Spectrum, J. Opt. Soc. Am., 53, 851-855, 1963.

Poschenrieder, W., Warneck, P., Gas Analysis by Photo-ionization Mass Spectrometry, Journal of Applied Physics, 37, 2812-2820, 1966.

Poschenrieder, W., Warneck, P., Mass Spectrometric Gas Analysis Utilizing Selective Photo ionization, , 40, 383-390, 1968.

Raffaelli, A., Saba, A., Atmospheric Pressure Photoionization Mass Spectrometry, Mass Spectrometry Reviews, 22, 318-331, 2003.

Revel'skii, I., Yashin, Y., Mass Spectrometry with Photoionization at Atmospheric Pressure and the Analysis of Multicomponent Mixtures Without Separation, Chemical and Physicochemical Methods of Analysis, 243-248, 1991.

Robb, D., Bruins, A., Atmospheric Pressure Photoionization (APPI): A New Ionization Method for Liquid Chromatography- Mass Spectrometry, US Patent 6,534,765 B1, 2003.

Robb, D., Covey, T., Bruins, A., Atmospheric Pressure Photoionization: An Ionization Method for Liquid Chromatography - Mass Spectrometry, Anal. Chem, 72, 3653-3659, 2000.

Sabine, G., Reflectivities of Evaporated Metal Films in the Near and Far Ultraviolet, 55, 1064-1069, 1939.

Schneider, E., Optical Properties of Lithium Fluoride in the Extreme Ultraviolet, The Physical Review, 49, 341-345, 1936.

Sieck, L., Gorden, R., Photoionization of Simple Hydrocarbons at 73.6-74.4 and 58.4 nm. Comparison with Penning Ionization, Chemical Physical Letters, 19, 509-512, 1973.

Syage, J., Real-Time Multispecies Monitoring by Photoionization Mass Spectrometry, US Patent 5,808,299, 1998.

Syage, J., Mechanism of $[M+H]^+$ Formation in Photoionization Mass Spectrometry, J. Am Soc Mass Spectro, 15, 1521-1533, 2004.

Syage, J., Evans, M., Hanold, K., Photoionization Mass Spectrometry, American Laboratory, 2000.

Syage, J., Hanning-Lee, M., Hanold, K., A Man-Portable, Photoionization Time-of-Flight Mass Spectrometer, Field Analytical Chemistry and Technology, 204-215, 2000.

Syage, J., Hanold, K., Rapid Response Mass Spectrometer, US Patent 6,326,615 B1, 2001.

Syage, J., Hanold, K., Lynn, T., Horner, J, Atmospheric Pressure Photoionization II. Dual Source Ionization, J. Chrom. A, 1050, 137-149, 2004.

Syage, J., Cai, S., Li, J., Evans, M., Direct Sampling of Chemical Weapons in Water by Photoionization Mass Spectrometry, Anal. Chem., 78, 2967-2976, 2006.

Takáts, Z., Wiseman, J., Gologan, B., Cooks, R., Mass Spectrometry Sampling Under Ambient Conditions with Desorption Electrospray Ionization, Science, 306, 471-473, 2004.

Tanaka, Y., Continuous Emission Spectra of Rare Gases in the Vacuum Ultraviolet Region, J. Opt. Soc. Am., 45, 710- 713, 1955.

Tanaka, Y., Jursa, A., LeBlanc,F., Continuous Emission Spectra of Rare Gases in the Vacuum Ultraviolet Region II Neon and Helium, Journal of the Optical Society of America, 48, 304-

308, 1958.

Venter, A., Nefliu, M., Cooks, G., Ambient Desorption Ionization Mass Spectrometry, Trends in Analytical Chemistry, 27, 284-290, 2008.

Walker, W., Samson, J., Rustgi, O., Optical Properties of Al for hv between 10 and 26 eV, Journal of the Optical Society of America, 48, 71, 1958.

Webb, J., Analytical Photoionization Mass Spectrometer with an Argon Gas Filter Between the Light Source and Monochromator, US Patent 3,521,054, 1970.

Wilkinson, P., Tanaka, Y., New Xenon-Light Source for the Vacuum Ultraviolet, Journal of the Optical Society of America, 45, 344-349, 1955.

Wood, R., Optical Properties of Homogeneous and Granular Films of Sodium and Potassium, Philosophical Magazine, 38, 98- 112, 1919.

Yamakita, Y., Yamauchi, M., Ohno, K., Penning Ionization Electron Spectra of Pyrene, Chrysene, and Coronene in Collision with Metastable He(2 ^{3}S) Atoms in the Gas Phase, Journal of Chemical Physics, 130, 24306, 2009.

Yamane, M., Photoionization Detector for Gases and Vapours, US Patent 3,454,828, 1969.